Accepted for publication in Coastal Engineering

Irregular wave runup statistics on plane beaches: application of a Boussinesq-type model incorporating a generating-absorbing sponge layer and second-order wave generation

Colm J. Fitzgerald, Paul H. Taylor, Jana Orszaghova, Alistair G. L. Borthwick, Colin Whittaker, Alison C. Raby

http://dx.doi.org/10.1016/j.coastaleng.2016.04.019

Irregular wave runup statistics on plane beaches: application of a Boussinesq-type model incorporating a generating-absorbing sponge layer and second-order wave generation

Colm J. Fitzgerald[a,*], Paul H. Taylor[a], Jana Orszaghova[b], Alistair G. L. Borthwick[c], Colin Whittaker[d], Alison C. Raby[d]

[a] *Department of Engineering Science, University of Oxford, Oxfordshire OX1 3PJ, UK*
[b] *HR Wallingford, Howbery Park, Wallingford, Oxfordshire OX10 8BA, UK*
[c] *School of Engineering, The University of Edinburgh, The King's Buildings, Edinburgh EH9 3JL, UK*
[d] *School of Marine Science and Engineering, Plymouth University, Drake Circus, Plymouth PL4 8AA, UK*

Abstract

Efficient absorption of reflected waves at the offshore boundary is a prerequisite for the accurate physical or theoretical modelling of long-duration irregular wave runup statistics at uniform, gently sloped beaches. This paper presents an implementation of the method suggested by Zhang et al. (2014) to achieve reflected wave absorption and simultaneous generation and propagation of incident waves in an existing numerical wave flume incorporating a moving boundary wavemaker. A generating-absorbing layer is incorporated within this 1DH hybrid Boussinesq-nonlinear shallow water equation model such that inshore-travelling incident waves, encompassing bound-wave structure approximately correct to second order, propagate unhindered while offshore-travelling reflected waves are absorbed. Once validated, the method is used to compile random wave runup statistics on uniform beach slopes broadly representative of dissipative, intermediate, and reflective beaches. Analyses of the individual runup time series, ensemble statistics and comparison to an empirical formula based on experimental runup data suggest that the main aspects of runup observed in the field are properly represented by the model. Existence of an upper limit on maximum runup is investigated using a simple extreme-value statistical analysis. Spectral saturation is examined by considering ensemble-averaged swash spectra for three representative beach slopes subject to incident waves with two different offshore significant wave heights. All spectra show f^{-4} roll-off at high frequencies in agreement with many previous field studies. The effect is also investigated of the swash motions preceding one particular extreme runup event on the eventual maximum runup elevation.

*Corresponding author
Email address: colm.fitzgerald@eng.ox.ac.uk (Colm J. Fitzgerald)

Keywords: Wave runup; Beaches; Irregular waves; Computational methods; Boussinesq equations

1. Introduction

Understanding and prediction of extreme runup events during periods of energetic irregular wave incidence on beaches is crucial for the planning and protection of new and existing coastal communities. The maximum wave runup level defines the boundary of the region of wave action which directly affects onshore sand transport, deposition and erosion and is of obvious importance in planning coastal setback distances or assessing coastal flooding probabilities. However, difficulties persist in identifying the cause and effect of near-shore phenomena due to the inherently nonlinear physics of wave hydrodynamics and continuously changing environmental conditions in the surf and swash zones.

Irregular wave runup, defined here as the time-varying shoreline vertical elevation, is typically separated into the wave setup component (time-averaged shoreline elevation relative to mean water level) and the swash oscillations about this setup level. Shoreline setup typically varies over time-scales of the order of 100 s at full scale and is rather difficult to measure accurately *in situ* where significant variations in beach morphology may occur on similar time scales. As an instantaneous quantity, swash is generally more straightforward to measure and a significant proportion of the literature on runup focuses on swash motions. Analysis of swash measurements obtained from field studies have been reported for intermediate beaches with local foreshore slopes between approximately 1/40 and 1/20 (cf. e.g. Guza and Thornton (1982) and Raubenheimer et al. (1995)), dissipative beaches with foreshore slopes less than 1/40 (cf. e.g. Ruessink et al. (1998) and Ruggiero et al. (2004)) and steeper, reflective beaches with slopes of order 1/10 (cf. e.g. Raubenheimer and Guza (1996)). Saturation of swash energy spectra at wind-wave frequencies and the absence of saturation at infragravity frequencies have been observed in many of these studies, e.g. Guza and Thornton (1982)and Raubenheimer and Guza (1996), although in highly dissipative conditions it has been noted that saturation can occur at shorter infragravity frequencies (Ruessink et al., 1998; Ruggiero et al., 2004). This indicates that swash oscillations arising from incident irregular waves involve competing processes whose magnitudes may vary depending on beach slope and incident conditions.

Numerical and laboratory studies of irregular wave runup on beaches are relatively rare compared with field studies owing to contamination of runup measurements and predictions by re-reflections of otherwise outgoing waves at the offshore boundary (i.e. wavemaker in laboratory

studies). A significant experimental study of irregular wave runup on beaches of different slopes was reported by Mase and Iwagaki (1984) and Mase (1989). No attempt was made to address the issue of reflections. For beaches with gentle slopes, much of the energy from the linear components of the incident wave train is dissipated through breaking and bed friction. Reflected energy in the linear frequency range can be adequately absorbed using force feedback control of the paddle. However, both the second-order bound long waves, which are non-negligible for energetic wave groups, and the offshore propagating long free waves arising during breaking undergo significant reflection at the offshore boundary. Despite advances in active-absorption wavemaker theory (Spinneken and Swan, 2009), it is still extremely difficult to absorb reflected long waves in laboratory flumes. Wavemaker reflections of otherwise outgoing long waves may compromise runup measurements and computations, just as spurious long waves generated at the paddle were observed to exaggerate runup and overtopping estimates in a numerical study by Orszaghova et al. (2014). Reliable estimates for runup necessitate the use of relatively short irregular wave trains to minimise interference from re-reflected waves.

In this paper, we seek to simulate long duration time series of irregular wave runup events using a hybrid Boussinesq-type model, an overview of which is presented in Section 2. This numerical wave flume, developed by Orszaghova et al. (2012), models wave evolution in one horizontal dimension and includes an in-built piston wavemaker. In order to eliminate wavemaker boundary re-reflection, we have modified the numerical model to incorporate sponge layer damping terms in the governing equations. Numerous applications of sponge layer absorption zones to Boussinesq-type numerical models appear in the literature, e.g. Larsen and Dancy (1983), Wei et al. (1999) and Madsen et al. (1997a), often in combination with an internal wave generator. Moreover, Madsen et al. (1997b) describe numerical simulations of experimental tests in an irregular wave runup study using such a configuration. Here, a generating-absorbing sponge layer is introduced similar to that described by Zhang et al. (2014) (also described by Siddorn (2012) in an ocean engineering context). Irregular wave propagation in the Boussinesq region is solved separately and imposed as a solution on a sponge layer in the full simulation of the wave runup problem. Thus, reflected waves are damped out completely while incident waves propagate accurately propagated inshore as demonstrated in Section 3. The distinct advantage of this method is its ability to propagate incident waves with approximately correct second-order bound harmonics, using a simplified wavemaker theory based on that derived by Schäffer (1996), while fully absorbing the reflected waves. Combined generation and absorption using relaxation zones has previously been proposed for Boussinesq methods by Bingham and Agnon (2005).

Using this adapted numerical wave flume, swash spectra for large ensembles of irregular wave runup simulations are obtained for two different significant wave heights on uniform bed slopes representing reflective, intermediate and dissipative beaches as reported in Section 4. Analysis of these swash spectra clearly shows the influence of beach slope on the swash spectra thus confirming previous observations in the field. Saturation of runup and the nature of the extreme runup are also investigated in Section 4 by examining the distribution of runup maxima with particular focus on the extreme event. Furthermore, an investigation into the effects of precursor bore motions at the shore on extreme runup events is also presented utilising the sponge layer.

2. Existing numerical model

A hybrid model of a shallow water flume, incorporating enhanced dispersion Boussinesq equations and nonlinear shallow water (NLSW) equations in one horizontal dimension is used to describe the generation, propagation, shoaling, breaking, and runup of incident irregular waves on a plane beach. The enhanced dispersion Boussinesq equations, derived by Madsen and Sørensen (1992), are employed to model the propagation and shoaling of weakly nonlinear, weakly dispersive waves from moderately deep water to the breaker line. When waves propagate into shallower water, the effects of nonlinearity become significantly greater than those of frequency dispersion and it is necessary to switch to the more appropriate nonlinear shallow water equations. The propagation of broken waves (modelled as bores) in the surf zone and the wetting and drying at the shoreline are naturally described within a Godunov-type finite volume framework. In particular, evolution of weakly discontinuous solutions of the NLSW equations (e.g. bores propagating up the beach) can be modelled using the shock-capturing capability of such finite volume schemes. Wave generation is achieved by implementation of a moving boundary piston paddle through the introduction of a local mapping of the time-varying physical domain in the vicinity of the paddle referred to as the paddle domain. A second-order wave generation methodology based on the theory derived by Schäffer (1996) provides the motion of the piston boundary. Finally, the switch between the Boussinesq and NLSW equations is determined from the current breaking location, identified from the most offshore wave where the local free-surface slope exceeds a prescribed threshold.

Numerical implementation of the hybrid solver is described in detail by Orszaghova et al. (2012) — a brief summary suffices for the purpose of this work. Solution in the Boussinesq region is obtained via a finite difference scheme involving centred five-point stencils. A fourth-order Runge-Kutta method is employed to advance the Boussinesq solution in time. In the shallow-water

region, a Godunov-type finite volume method with HLLC approximate Riemann solver is used to discretise the hyperbolic formulation of the NLSW equations. Second-order accuracy in time and space is obtained using the MUSCL-Hancock predictor corrector scheme. The solution scheme switches from a finite difference to a finite volume method according to the ad hoc breaking initiation criterion. A threshold free surface slope value of $-\eta_x \geq 0.4$ was found by Orszaghova et al. (2012) to be sufficient for all validation cases. The breaking front is tracked inshore by recalculating the breaking location at each time step. A local movable grid, which varies from being fully Lagrangian at the paddle face to fully Eulerian away from the paddle, discretises the paddle domain and is mapped onto the fixed Eulerian grid and the governing equations are solved on this grid. Special treatment of the finite difference equations (by inclusion of time-varying parameters) on the mapped grid points is also necessary to ensure accurate modelling of the moving boundary wavemaker. More details regarding the moving boundary wave generator can be found in § 2.6 and § 3.2 of Orszaghova (2011).

An obvious limitation of the present numerical model compared to other Boussinesq-type models is the weakly nonlinear approximation inherent in the enhanced dispersion equations. More sophisticated numerical models exist (e.g. Shi et al. (2012) and Tissier et al. (2012)) which utilise the 'fully nonlinear' Boussinesq equations (of Chen (2006) and Green and Naghdi (1976), respectively). A further limitation of the present numerical model is that all waves inshore of the most offshore breaking point are treated with the NLSW equations. Consequently, the influence of frequency dispersion on smaller waves inshore of a large breaker is neglected by the present breaking algorithm. Tissier et al. (2012) noted that many hybrid Boussinesq-NLSW models do not allow the termination of breaking, thus making them unsuitable for irregular wave transformations over uneven bathymetries. Both Tissier et al. (2012) and Tonelli and Petti (2012) introduce criteria to allow the governing equations to switch from Boussinesq to NLSW and also to revert from NLSW to Boussinesq so that the tracking of individual breaking wave fronts is possible. However, in surf zones of moderate length, such as those considered herein, the effect of neglecting frequency dispersion for small waves inshore of large broken waves on the shoreline dynamics is likely to be small. Therefore, the model described here provides a sensible balance between accuracy and computational speed – an important factor when collecting large sets of runup statistics.

3. Irregular wave runup using generating-absorbing sponge layerl

3.1. Incorporation of sponge layer in existing model

In the present model, the in-built moving boundary piston paddle allows accurate reproduction of wave flume experiments involving piston-type wavemakers. In fact, if the experimental wavemaker moves subject to displacement control then the same paddle signal could be used as input to the numerical wave flume. Evanescent fields arising in the vicinity of a piston wavemaker will differ significantly in the physical wave flume compared with the Boussinesq numerical wave flume where the assumption of fairly shallow water leads to small or negligible evanescent mode contributions. A full second-order wave generation theory for the enhanced dispersion Boussinesq equations of Madsen et al. (1991) would require a new derivation based on the bound wave theory of Madsen and Sørensen (1993). As an approximation, a simplified version of the full Stokes-wave theory of Schäffer (1996) is adopted wherein all evanescent mode contributions are neglected. Schäffer (1996) concluded that substantial errors would not be introduced by neglecting evanescent mode contributions provided the waves are in the intermediate or shallow water depth regime. This, of course, is the regime appropriate for the Boussinesq description of wave propagation and so evanescent-free second-order wavemaker theory (similar to the approach described by Barthel et al. (1983)) is adopted.

Nevertheless, the numerical wave flume suffers from the same disadvantages as its physical counterpart, in particular the difficulty in absorbing long waves reflected at the beach and those long free waves released at breaking. In a recent numerical investigation involving the model described in Section 2, Orszaghova et al. (2014) emphasised the importance of generating the correct long wave bound harmonic structure for runup and overtopping estimates. In certain laboratory flumes, effective absorption of otherwise re-reflected waves in the linear incident frequency range has been achieved using active wave absorption (based on force feedback or free-surface elevation feedback control). Higuera et al. (2015) recently implemented such active absorption in a numerical context. However, we seek to model irregular wave runup in cases where the incident irregular wave field is approximately accurate to second-order so that outgoing reflected and free waves outside the linear frequency range must also be absorbed. Noting that we require wave absorption over the entire incident frequency spectrum, including sum and difference frequencies, we adopt a sponge layer damping zone.

Inclusion of both a sponge layer damping zone (no corresponding physical mechanism) and a moving boundary wavemaker (modelling a physical wavemaker) is self-contradictory from the

perspective of modelling either field conditions or a laboratory wave flume. However, the moving boundary wavemaker in the existing model has been extensively validated (see Orszaghova et al. (2012) for details) and serves purely to generate an approximately correct second-order field in modelling irregular wave runup. In a model with an offshore boundary inlet condition the same approach (described below) may be adopted without apparent incompatibility of the wave generation and absorption mechanisms. Section 3.2 provides further discussion of the limitations of combining a moving boundary wavemaker with a generating-absorbing sponge layer.

The sponge layer approach was originally proposed by Israeli and Orszag (1981) for a general wave system, and has proved widely effective at absorbing outgoing waves of different celerities. Larsen and Dancy (1983) pioneered its use in shallow water Boussinesq-type modelling for the absorption of backward-generated (from a free-surface source function) and reflected waves. The additional sponge-layer absorption terms in the mass and momentum/energy conservation equations yield proportional control of the solution that tends towards zero disturbance over the extent of the sponge layer. Recently, Zhang et al. (2014) also recognised the possibility of implementing wave generation as well as absorption in Boussinesq-type equations. Independently, Siddorn (2012) also proposed a modification of the sponge-layer damping approach in a fully nonlinear potential flow model to allow simultaneous wave generation and absorption. The implementation adopted herein broadly follows that of Zhang et al. (2014), as summarised below. A combined generating-absorbing sponge layer approach with second-order wave generation has not been implemented in a numerical wave flume before for the purposes of irregular wave runup modelling, as far as we are aware. By implementing these existing methods together in a Boussinesq-NLSW model, it is possible to conduct simulations of irregular wave runup at enhanced accuracy.

To achieve wave damping across the sponge layer, the continuity and momentum equations from the enhanced dispersion Boussinesq equations, formulated in terms of the free-surface elevation above a prescribed horizontal datum ($\eta = b + h + \zeta$) and depth-integrated velocity $q = q(x,t)$, are modified by sponge layer damping terms as follows

$$\eta_t + q_x = \alpha_{11}(x)(\eta_0 - \eta), \tag{1}$$

$$q_t + \left(\frac{q^2}{d} + \frac{1}{2}g(\eta^2 - 2\eta b)\right)_x = -\tau_b/\rho - g\eta b_x + (B + 1/3)h^2 q_{xxt} + Bgh^3\eta_{xxx}$$
$$+hh_x(q_{xt}/3 + 2Bgh\eta_{xx}) + \alpha_{12}(x)(q_0 - q) - \alpha_2(x)/h^2(q_0 - q)_{xx}. \tag{2}$$

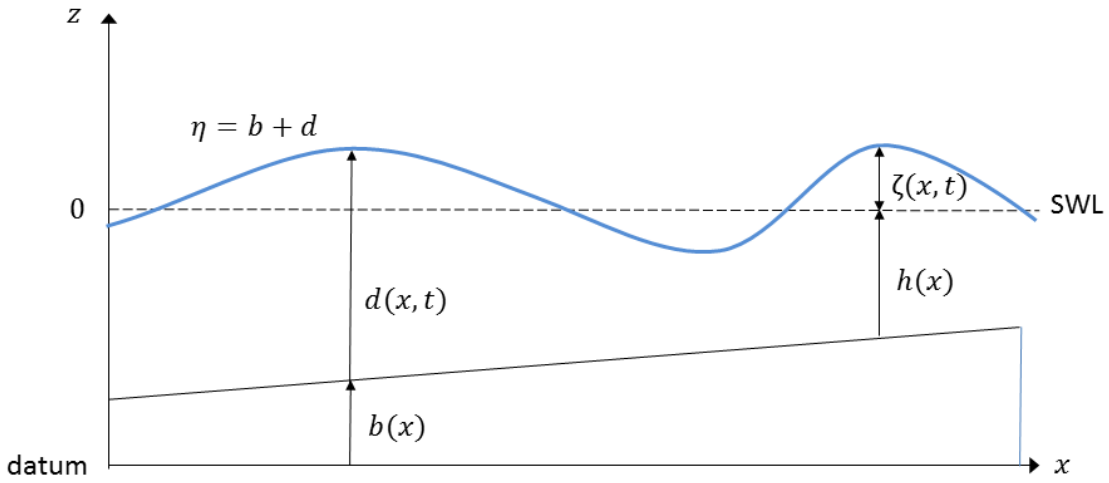

Figure 1: Definition sketch (Orszaghova et al., 2012)

.

where (α_{11}, α_{12}, α_2) are the damping strength functions and (η_0, q_0) are the imposed solutions. Other variables and parameters appearing in these equations include: the still water depth $h = h(x)$; the local total water depth $d = d(x, t)$; acceleration due to gravity g; free linear dispersion parameter for enhancing dispersion characteristics $B = 1/15$, and quadratic bottom friction, included through the τ_b term. Figure 1 depicts the depth and free-surface elevation variables. The $(\alpha_{11}, \alpha_{12})$ sponge-layer terms correspond to what Wei and Kirby (1995) call "Newtonian cooling" terms and occur in both mass continuity and momentum equations. The damping coefficients in the continuity and momentum conservation equations can be assumed to be equal, noting that Siddorn (2012) and Zhang et al. (2014) found that setting $\alpha_{11}(x) = \alpha_{12}(x) = \alpha_1(x)$ yielded good absorption properties. The second damping term in Equation (2) is diffusive in nature, similar to the linear viscous damping term in the Navier-Stokes equation. For $q_0 = 0$ it is necessary for this term to be positive to yield dissipation of the wave energy through diffusion.

The traditional sponge layer damping condition is recovered by setting the imposed free-surface elevation η_0 to the still water level, i.e. $\zeta_0 = 0$ and $q_0 = 0$. However, if the imposed solution $(\eta_0(x, t), q_0(x, t))$ is an incident wave solution of the enhanced dispersion Boussinesq equations then the total wave will be damped towards this incident wave on the sponge layer. Therefore in the absence of other wave disturbances the sponge layer will *generate* an incident wave whereas if, for example, a wave disturbance comprising incident and reflected components enters the sponge layer the reflected wave will be *absorbed*. The imposed solution can be linear or nonlinear, and

can encompass regular or irregular waves. However, to avoid propagation of error waves outside the sponge layer it is most useful to use solutions of the homogeneous (undamped) governing equations. In a numerical context, such solutions can be obtained directly from an existing numerical solution if no analytical expression exists.

The $\alpha_1(x)$ terms in both mass and momentum conservation equations, dominate the damping control so that $\alpha_2(x)$ is not strictly necessary, as will be demonstrated by means of numerical examples. The width of the sponge layer L_s is typically assumed to be one or two wavelengths. Although longer sponge layers are preferable to minimise reflections, it has proved necessary to specify a relatively compact sponge layer in the irregular wave simulations (discussed in Section 4). The spatial profile $f(x)$ of the sponge layer is location-dependent. If the sponge layer is situated at the edge of the computational domain then a monotonically increasing function from the interior to the edge suffices. If the sponge layer is not contiguous with the domain boundary then a symmetrically increasing/decreasing profile about the mid-point of the sponge layer should provide good absorption properties. Zhang et al. (2014) found little difference between linear and quadratic profile functions and so linear profiles are assumed hereafter. Following the convention adopted by Zhang et al. (2014), the sponge layer functions are given by $\alpha_1(x) = \tilde{\alpha}_1 f(x)$ and $\alpha_2(x) = \tilde{\alpha}_2 f(x)$, where $\int_0^{L_s} f(x)\,dx = 1$ so that $\tilde{\alpha}_1$ and $\tilde{\alpha}_2$ denote the integrated sponge layer strengths.

3.2. Irregular wave modelling – coupled simulations

The generating-absorbing sponge layer is utilised to simulate long periods of irregular wave incidence on a beach using the following method, similar to the nested domain approach demonstrated by Zhang et al. (2014). Assume the simulation domain consists of a piston wavemaker at the left end of the tank, a flat-bed section, wherein a generating-absorbing sponge layer is placed, followed by a plane beach of uniform bed slope extending from the beach toe through the still water level and beyond as illustrated in the lower diagram in Figure 2. An offshore incident wave field $(\eta_0(x,t), q_0(x,t))$ is imposed each time step on the sponge layer offshore of the beach so that simultaneous absorption of reflected outgoing waves and propagation of incident waves is achieved. Any outgoing reflected wave components which interact with incident waves between the shore and the sponge layer are damped out within the sponge layer. The incident wave field offshore of the beach is determined by simulation of incident wave propagation in the absence of beach reflections. The incident wave propagation computational domain must have an identical flat-bed offshore geometry to the irregular wave runup domain which is continued inshore instead of the

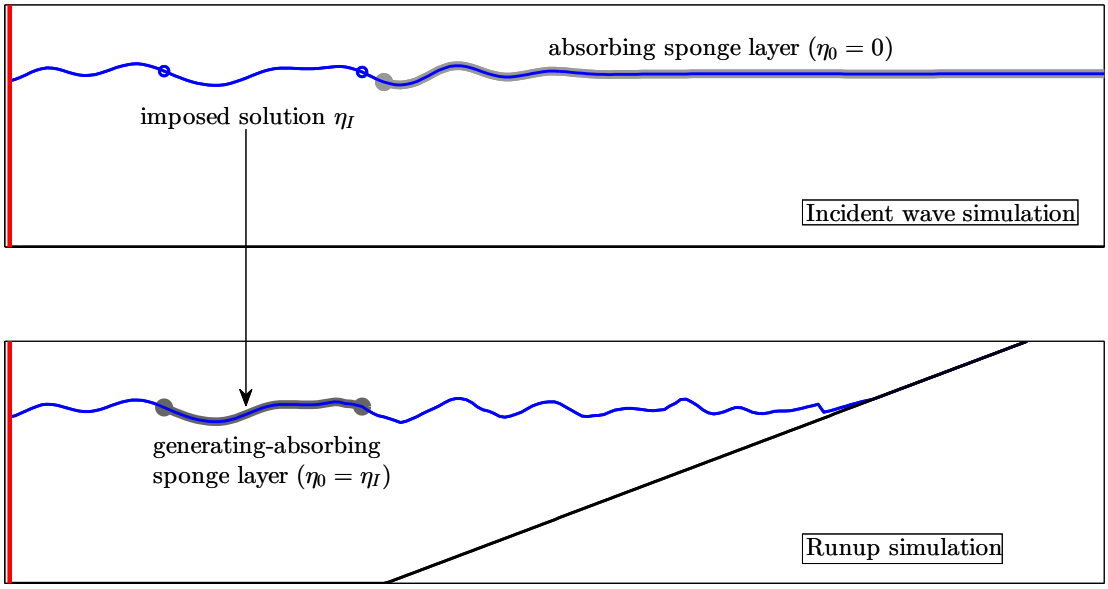

Figure 2: Illustration of coupled incident irregular wave and beach runup simulations showing 'nested' solution range.

beach as represented in the upper and lower panels of Figure 2, respectively. A long absorbing sponge layer situated immediately in front of the right-hand domain boundary is introduced to prevent beach reflections contaminating the incident wave signal, as shown in the upper panel of Figure 2.

In practice, the coupled incident wave propagation and beach runup simulation is implemented as follows. The same values of basic parameters (tank length L, still water depth on the flat bed h_{SW}, number of grid points N, time step Δt) are used in both simulations. Identical wavemaker paddle signals are prescribed (although this may not be strictly necessary as the sponge layer can itself generate waves). Nevertheless, given the relatively compact nature of the sponge layer it would be challenging to generate accurately the total incident wave disturbance from still water using proportional sponge-layer control. Instead, we seek solely to absorb the outgoing reflected wave component of the total wave signal. At each time step the incident wave solution is determined first, providing input for the sponge layer in the beach runup simulation, and then the beach runup solution is obtained.

Presence of a moving boundary wavemaker and associated paddle domain complicate the imposition of the sponge layer boundary condition. Mappings between the physical and computational paddle domains (modelling expansions and contractions of the physical locations of the

grid points) introduce extra terms in the enhanced dispersion Boussinesq equations (Orszaghova et al., 2012) and so it is more straightforward to restrict the sponge layer boundary conditions to the region beyond the paddle domain. Consequently, in the runup simulation the sponge layer is placed between the end of the paddle domain and the beach toe. The beach toe provides a natural shoreward limit for the sponge layer because the beach is omitted from the incident wave simulation. The absence of the beach in the incident wave domain is necessary to avoid any reflections from the beach, as these would be re-reflected by the wavemaker causing contamination of the incident wave field. Therefore, the wave field obtained from the incident wave simulation inshore of the beach toe cannot be utilised in the full simulation.

As noted in Section 3.1, a fixed-position wavemaker which fluxes waves through the offshore boundary could be used to generate the incident wave field and would have the advantage of allowing an extended generating-absorbing sponge layer. However, the generating-absorbing sponge layer is efficient even when quite compact and so any small outgoing long waves will be sufficiently damped in the region between the paddle domain and beach toe. An alternative formulation would involve directly imposing the analytical second-order solution derived by Madsen and Sørensen (1993) for the enhanced dispersion Boussinesq equations on the sponge layer, and so utilising the generation capabilities of the sponge layer. Generation of a second-order wave field from still water would require a stronger sponge layer than is necessary for simply absorbing reflected waves; however, imposition of the second-order incident wave field over the sponge layer on an incident linear field propagating from the offshore boundary would be a viable alternative.

To verify the foregoing coupled incident wave propagation/irregular wave runup method for modelling irregular wave-incidence on a beach it is necessary to determine damping coefficients that minimise sponge layer reflections and transmissions. Absorption characteristics of the sponge layer are investigated for both focused wave group and regular waves incidence. The spectrum from which the components of the focused wave group are determined and from which the frequencies of the regular waves are selected is identical to the incident wave spectrum used in the irregular wave runup simulations, the results of which are presented in Section 4.

3.3. Sponge layer performance

In the simulations to be presented in Section 4, we seek to damp out reflections of broad-banded incident wave-trains while propagating the incident wave-trains over a compact sponge layer. In this context, it is useful to first consider reflected and transmitted waves due to focused wave group propagation over a sponge layer of width equal to two peak wavelengths. A typical value

of the integrated damping strength $\tilde{\alpha}_1$ which yields good absorption is given by 4ω as observed in regular wave tests for incident waves of frequency ω for sponge layer widths of one or two wavelengths. Similar values for $\tilde{\alpha}_2$ are also specified – although given the $1/h^2$ term it is more difficult to specify a damping strength providing satisfactory absorption properties in general.

The computational domain geometry is chosen to be typical of shallow water flumes found in many experimental facilities. Thus, the still water depth at the paddle was chosen to be $h_{SW} = 0.5\,\mathrm{m}$. The energy density spectrum of the incident focused wave group corresponds to that implemented by Hunt (2003), Hunt-Raby et al. (2011) and Borthwick et al. (2006) in a series of experimental studies of focused wave group runup and overtopping. It is a truncated Pierson-Moskowitz spectrum with peak frequency $f_p = 0.464\,\mathrm{Hz}$, upper and lower cut-off frequencies of $f_{min} = 0.330\,\mathrm{Hz}$ and $f_{max} = 0.964\,\mathrm{Hz}$, respectively, and discretised into $N = 53$ equally spaced components. With a corresponding peak wavelength of $\lambda_p = 4.43\,\mathrm{m}$, the specified computational domain length $L = 36\,\mathrm{m}$ allows reflection and transmission regions of three wavelengths in extent on either side of the sponge layer located on the interval $(12.0\,\mathrm{m}, 21.0\,\mathrm{m})$. A linear focus amplitude of $0.0570\,\mathrm{m}$ is selected, the smallest from the range of linear focus amplitudes utilised in the tests of Hunt (2003), etc., and the linear focus location is prescribed at the centre of the domain $x_f = 16.5\,\mathrm{m}$. Precise details of the focused wave shape are provided in Section 5 of Orszaghova et al. (2012). Given that beach reflected waves comprise a fraction of the total incident wave energy to be damped, this moderately-sized incident wave is considered a reasonable test for the damping effects of the sponge layer. A frictionless flat bed is considered, in order to model damping due solely to the sponge layer. Solutions were found to have converged for a uniform grid spacing Δx of 0.02 m and a time step Δt of 0.004 s.

Three different pairs of integrated damping strengths $(\tilde{\alpha}_1, \tilde{\alpha}_2)$ are considered for a sponge layer width of approximately two peak wavelengths. The first two cases, $(\tilde{\alpha}_1, \tilde{\alpha}_2) = (4\omega_p, 4\omega_p)$ and $(8\omega_p, 8\omega_p)$, involve equal 'Newtonian cooling' and 'viscous' damping strengths. In the third case, only the proportional or 'Newtonian cooling' damping term is non-zero $(\tilde{\alpha}_1, \tilde{\alpha}_2) = (4\omega_p, 0)$. The sponge layer lies in the interval (12.0 m, 21.0 m). Free surface elevation time series of the reflected and transmitted wave components are recorded at $x = 11.0$ m and $x = 22.0$ m equidistant from the focus location. Reflected waves are obtained by subtracting the incident wave field, computed in a different simulation, from the total wave field. In the incident wave simulation, the central sponge layer is removed and replaced by a sponge layer extending four wavelengths inwards from the right hand boundary of the numerical wave flume. Integrated damping strengths of $(\alpha_1, \alpha_2) = (4\omega_p, \omega_p)$ yield negligible reflection and effectively total absorption.

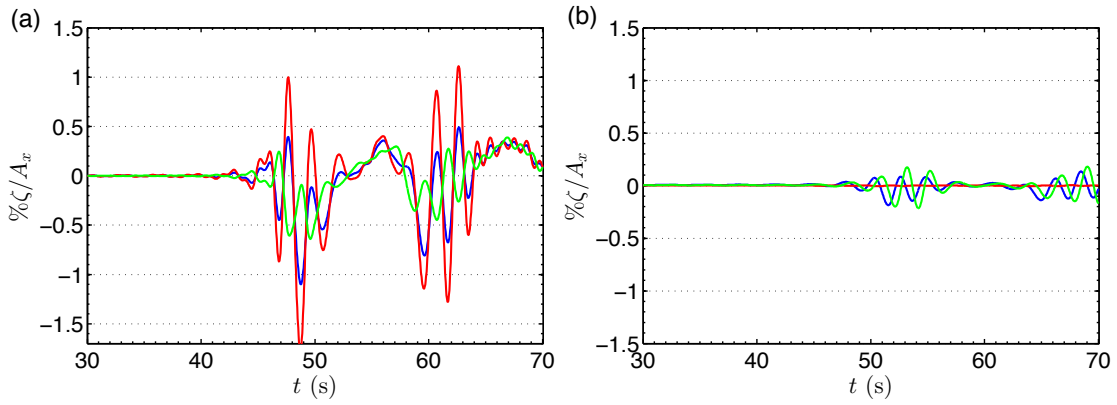

Figure 3: (a) Reflected and (b) transmitted wave free-surface displacement time histories as percentages of the linear wave amplitude A_x at the measurement locations for integrated damping strengths $(\alpha_1, \alpha_2) = (8\omega_p, 8\omega_p)$ (red), $(\tilde{\alpha}_1, \tilde{\alpha}_2) = (4\omega_p, 4\omega_p)$ (blue) and $(\tilde{\alpha}_1, \tilde{\alpha}_2) = (4\omega_p, \omega_p)$ (green).

Figure 3 shows the reflected and transmitted wave free-surface displacement time histories normalised by the focused wave envelope amplitude at the locations equidistant from the focus (so that defocusing effects are separated from sponge layer absorption). The effect of the viscous damping term can be seen by comparing the relative amplitudes of the reflected and transmitted waves for the three pairs of damping strengths considered. Although inclusion of the viscous damping term does reduce wave transmission, this appears to be at the expense of increased reflection. The optimal sponge layer specification from the three sets proposed is for $(\tilde{\alpha}_1, \tilde{\alpha}_2) = (4\omega_p, 0)$ where both reflected and transmitted wave amplitudes are less than 0.5% of the focused wave amplitude. Further tuning is possible ($\tilde{\alpha}_2 = \omega_p$ yields slightly smaller reflections) but the benefits are insubstantial. In the coupled simulations, it is inevitable that any beach-reflected or offshore-travelling free waves transmitted through the sponge layer towards the wavemaker will be damped upon re-entering the sponge layer after reflection at the wavemaker boundary. Minimising sponge layer reflection is thus significantly more important than minimising sponge layer transmission. Therefore, the viscous damping term is set to zero in most cases considered hereon.

Absorption performance of wall-adjacent sponge layers is usually assessed by measuring the reflection coefficient, i.e. reflected wave amplitude normalised by incident wave amplitude, over a range of frequencies, using a broad-banded irregular incident wave-field. An irregular incident sea state was realised from a top hat spectrum discretised into 119 frequency components over the frequency range (0.134 Hz, 0.855 Hz) using a random phase method. All components were specified to have equal amplitudes such that the significant wave height of the sea sate was

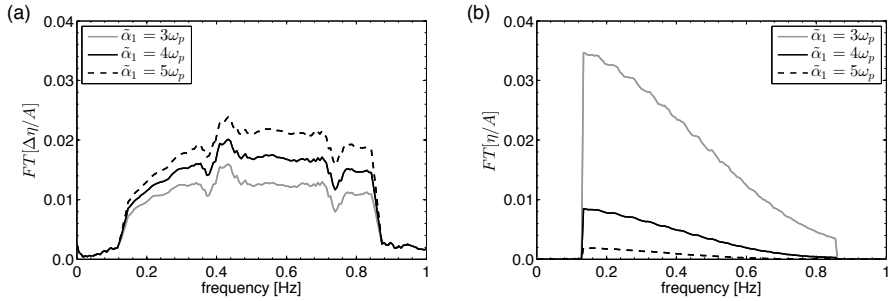

Figure 4: (a) Normalised reflection coefficient and (b) normalised transmission coefficient for a sponge layer of width $\lambda_p \simeq 4.5$ m subject to linear incident irregular waves randomly realised from a top hat spectrum spanning (0.134 Hz, 0.855 Hz).

$H_s = 0.001$ m, i.e. the incident wave is effectively linear. A generating sponge layer of width 15.0 m situated adjacent to the left-hand boundary propagated the incident waves towards a compact absorbing sponge layer of width 4.5 m (approximately one peak wavelength of the P-M spectrum) located 10 m from the generating sponge layer. The absorbing sponge layer had a triangular profile and three different integrated absorption strengths were considered ($\alpha_1 = 3\omega_p, 4\omega_p, 5\omega_p$); the diffusive absorption strength was set to zero. Reflected waves were obtained by subtracting the linear analytical incident wave solution (Madsen and Sørensen, 1993) from the total numerical solution between the generating and absorbing sponge layers. Figure 4 presents the normalised reflected and transmitted wave amplitude spectrum. The reflection spectrum was obtained by averaging the FFT of reflections at four locations between the generating and absorbing sponge layers. On the other hand, the normalised transmission amplitude spectrum was obtained from the FFT of the elevation at the right-hand boundary of the domain (located 10.0 m from the absorbing sponge layer). An integrated sponge layer strength of $\alpha = 4\omega_p$ yields reflections of less than 2% and transmissions of less than 1%. Transmission tends to increase with decreasing frequency a well-known property of sponge layers. Conversely, reflection amplitudes decrease with decreasing frequency (below 0.4 Hz at least). By extending the length of the sponge layer and keeping the integrated sponge layer strength constant it is possible to reduce reflections while maintaining very low transmission. Reflection amplitudes of 2% are deemed satisfactory for such a compact sponge layer and show that the combined use of moving boundary paddle and sponge layer does not seriously compromise the results.

3.4. Demonstration of an irregular wave runup simulation

This section provides a practical demonstration of the effectiveness of the coupled irregular wave propagation and beach interaction simulations. Rather than investigating the amplitudes of

reflected and transmitted waves outside the sponge layer (both of which would be difficult to isolate in a domain featuring incident and beach-reflected waves) the behaviour of the shoreline is used to assess the performance of the generation-absorption zone. In other words, if an irregular incident wave train of a given repeat period is simulated for, say, two repeat periods, then how good is the agreement between shoreline positions for each repeat period? Hence, a 'coupled' simulation of irregular wave incidence on a beach with a typical generating-absorbing sponge-layer configuration is considered next.

The energy spectrum for the irregular wave train is again based on one used in the UKCRF tests (Hunt, 2003). The spectrum is discretised into 157 components corresponding to a repeat period of approximately 245.76 s. The mean zero-crossing period of the sea state is approximately 1.75 s so that on average each repeat period comprises 140 waves. The significant wave height of the offshore spectrum is chosen to be $H_s = 0.10$ s corresponding to a steepness coefficient of $(H_s/\lambda_z) \simeq 0.03$ where λ_z is the wavelength associated with the mean zero-crossing period. Amplitudes and phases of the linear components of the random realisation of the sea state are obtained using the random-amplitude/random-phase method (Tucker et al., 1984), i.e. the amplitudes are determined from the Rayleigh distribution with scale parameter $\sqrt{S(f)\Delta f}$ and the phases from the uniform distribution on $(0, 2\pi)$, respectively. The second-order wavemaker signal comprising sub- and super-harmonics is computed based on the wavemaker theory of Schäffer (1996).

The computational domain geometry is based on the UKCRF wave basin: a beach with a 1:20 slope is present in the full runup simulation, extending from the beach toe located 8.33 m from the equilibrium position of the paddle to beyond the still water level. In the region between the paddle and the beach toe, the still water depth is 0.5 m. The paddle domain extent is approximately ten times the maximum paddle sweep (equal to approximately 0.25 m from Figure 5). Thus, the sponge layer is positioned in the flat-bed Boussinesq equation region between $x = 2.75$ m and $x = 8.25$ m, and is of width $1.25\lambda_p$. An integrated sponge layer strength of $\tilde{\alpha} = 4\omega_p$ is chosen based on the previous damping zone investigations. The grid spacing is 0.02 m and the time-step 0.004 s. A quadratic bed friction coefficient $C_f = 0.008$ is selected based on previous calibration tests. Irregular wave runup on the beach is simulated for two repeat periods, and the shoreline position records for each repeat period then compared.

Figure 5 shows both the first-order (erroneous) and second-order (corrected) wavemaker paddle signals over a single repeat period. It is evident that the paddle must undergo large excursions subject to the second-order wavemaker correction in order to eliminate the spurious long error

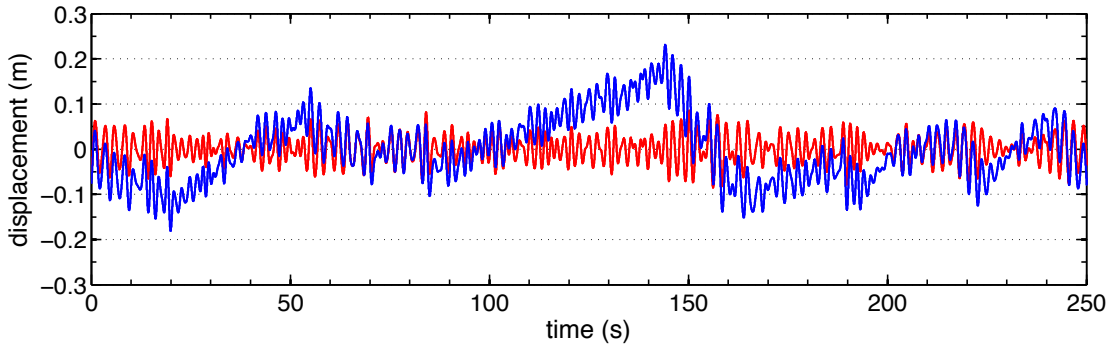

Figure 5: First-order (red) and second-order corrected (blue) wavemaker paddle displacement time histories for a random realisation of the UKCRF JONLSWAP spectrum, peak frequency $f_p = 0.464\,\mathrm{Hz}$ and significant wave height $H_s = 0.10\,\mathrm{m}$. See online version for colour.

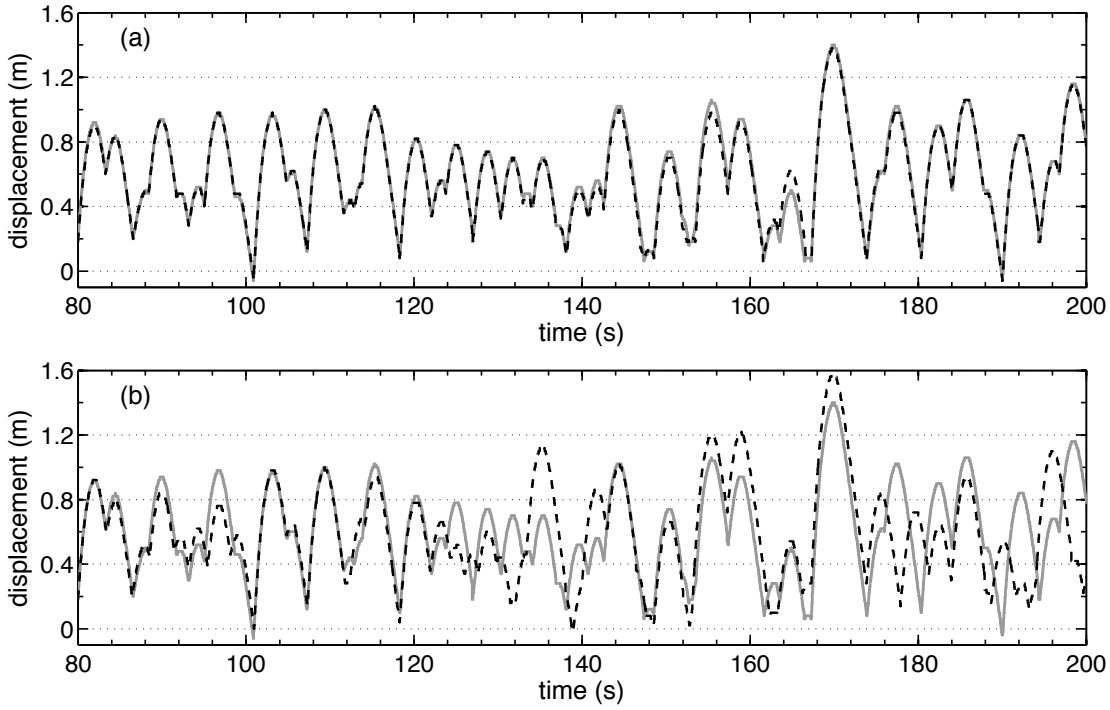

Figure 6: Shoreline displacement in the plane of the beach relative to the still water shoreline for corresponding intervals of the first repeat period (grey) and second repeat period (black, dashed) for damping strengths (a) $\tilde{\alpha}_1 = 4\omega_p$ and (b) $\tilde{\alpha}_1 = 0.3\omega_p$.

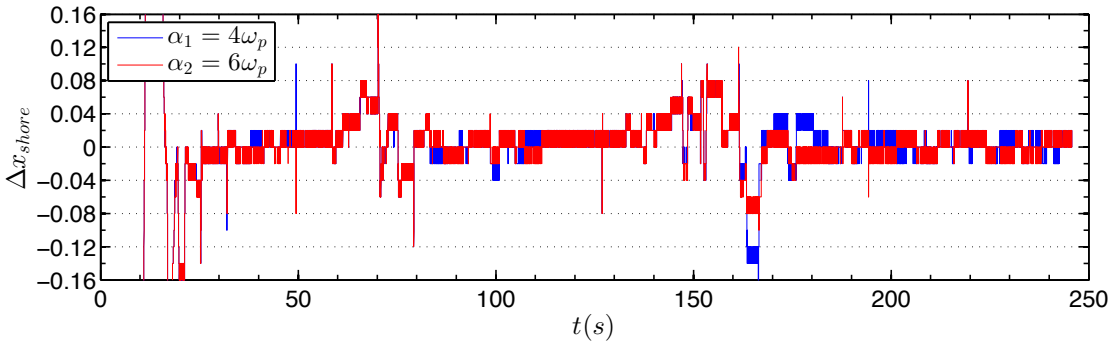

Figure 7: Difference between the displacement of shoreline in the plane of the beach relative to the still water shoreline 18.33 m from the paddle for first repeat period and second repeat period for two different absorption strengths $\tilde{\alpha}_1 = 4\omega_p$ (blue), $\tilde{\alpha}_1 = 6\omega_p$ (red).

waves arising from first-order theory, and so obtain the correct bound subharmonic structure. Figure 6 presents predicted shoreline motions resulting from second-order wave generation over two full repeat periods, with the signal for each repeat period overlaid for comparison purposes. The upper plot (a) is obtained for typical integrated sponge layer strength and the lower plot (b) for a very low integrated strength. In Figure 6 (a) the agreement between the shoreline motions over the first and second repeat period is good despite some minor discrepancies. There is no evidence that reflected energy is trapped because there is no trend towards larger or smaller motions during the second repeat period. However, small reflections at the sponge layer caused by outgoing long waves from the beach reflection may impinge on the shoreline motions almost equally for each repeat period. Nevertheless, the results are encouraging, particularly when compared to Figure 6 (b) where large variations are evident in the motions for each repeat period, and indicate that the present method is effective at simulating irregular wave runup.

Figure 7 shows the difference in shoreline displacement obtained over the first and second repeat periods as shown in Figure 6 (a). The discrete nature of the predicted shoreline motion is particularly evident in the shoreline difference time-history because the magnitude of the runup difference is not much larger than the shoreline step size $\Delta x = 0.02\,\mathrm{m}$ and so is affected by the wetting and drying algorithm. Beyond the initial start-up transient for the first repeat period, the shoreline positions are generally no further apart than two or three grid cells, thus revealing satisfactory agreement between the simulation predictions during the first and second repeat periods. It should be noted that discrete changes in the shoreline position time-history over time increments of $\Delta t = 0.004\,\mathrm{s}$ cannot be represented adequately in Figure 7 and give the time-history

plot a block-like appearance. Based on this comparison of the shoreline displacement differences for the sponge layer strengths $\alpha = 4\omega_p$ and $\alpha = 6\omega_p$, it appears the stronger sponge layer provides better repeatability and so is used as standard for all the following simulations.

4. Irregular wave runup simulations — results and analysis

Multiple numerical simulations of irregular wave runup on beaches are now used to assemble a comprehensive set of runup records for one incident spectral shape (with various target significant wave heights). Simple bulk and extreme-value statistical analyses are conducted on the ensembles of runup records. Qualitative comparison of the results with measured laboratory data should at least partially validate the numerical model. Several theoretical and empirical deficiencies in the 1DH hybrid model have been identified (see the discussion in Section 2), particularly with regard to nonlinear wave behaviour during shoaling and the mechanics of wave breaking, which might lead to inconsistencies between numerical predictions and physically-measured data. However, the model is fast and robust so that large datasets for statistical analysis can be constructed efficiently. It should be emphasised that the primary interest of the present investigation is not to model conditions and runup in the field as accurately as possible — instead it is to understand the processes that affect wave runup probability distributions (extreme or otherwise) under idealised conditions. Such conditions, where the beach slope is uniform in space and constant in time, are more representative of shallow water flume laboratory than field conditions. However, both existing field data and laboratory data are used as benchmarks for comparison with model results.

4.1. Simulation specifications

Figure 2 outlines the computational domain of the irregular wave runup simulation, where the still water depth is constant for a given distance inshore of the paddles, beyond which there is a beach of uniform slope. Irregular wave runup on the beach is characterised by the offshore wave spectrum (specified by its shape and the significant wave height H_s and peak period T_p parameters), offshore depth and beach slope. No other length-scales are needed.

4.1.1. Beach slopes

Uniform bed slopes of 1/10, 1/20 and 1/40 are considered with the intention that the slopes represent reflective, intermediate and dissipative beach types, respectively. In the literature, there is no precise consensus on what beach slopes correspond to what types; steep reflective beaches are sometimes considered to have slopes greater than 1/10. However, generally speaking,

dissipative gently sloping beaches have gradients less than 1/20 and reflective slope beaches are of order 1/10 and greater, as stated by Baldock et al. (1998). Care should be taken not to choose a very steep slope as the assumption of a slowly-varying bathymetry underlying the Boussinesq governing equations may be invalidated. The intermediate slope of 1/20 is often specified in laboratory wave flumes (Borthwick et al., 2006; Hunt-Raby et al., 2011). In addition to these three representative slopes, a slope of 1/30 is also considered when analysing the bulk statistics of runup in Section 4.2.1 although only a small ensemble of irregular wave runup records are gathered in this case.

4.1.2. Offshore spectrum and simulation times

The spectral shape, cut-off frequency, and peak frequency are identical to those specified in Sections 3.3 and 3.4for a Pierson-Moskowitz spectrum with $f_{min} = 0.330\,\text{Hz}$, $f_{max} = 0.964\,\text{Hz}$ and $f_p = 0.464\,\text{Hz}$. The still water depth between the paddle and the beach toe is $h = 0.5\,\text{m}$. A finer resolution discretisation of the wave spectrum is used to extend the existing (focused wave group) repeat period; by increasing the number of wave components in the incident wave-field from $N = 53$ to $N = 313$, the return period T_r is increased from 81.92 s to 491.52 s. The spectral zero-crossing period, defined as $T_z = \sqrt{m_0/m_2}$ where m_n is the n^{th} spectral moment computed over the truncated frequency range, is approximately 1.75 s so that one return period corresponds to approximately 280 waves. Significant wave heights H_s of less than 0.10 m are selected, corresponding to a maximum steepness parameter of $H_s/\lambda_p = 0.023$ based on the peak spectral component. This energy density spectrum represents a moderate sea state. Importantly, the associated piston paddle motions do not require extremely large paddle domains and the sponge layer extent in most cases is at least one wavelength.

The grid spacing (finite difference) or cell size (finite volume) is 0.02 m and the time step is 0.002 s. Domain lengths of 18 m, 24 m and 32 m are specified for the beach slopes of 1/10, 1/20 and 1/40, respectively. The beach toe is located 8.33 m from the zero excursion paddle position. The total simulation time is specified to be $1.2T_r$ to prevent any start-up transient effects from contributing to the runup statistics. One complete runup simulation constitutes 150,000 time steps (for both incident wave propagation and incident wave runup simulations). The total CPU time taken on a standard desktop computer (Intel®Xeon®W3540 2.93GHz processor with 6.00Gb RAM) is about 15 minutes for the two parts of the coupled runup simulation on a domain of 1200 spatial grid points.

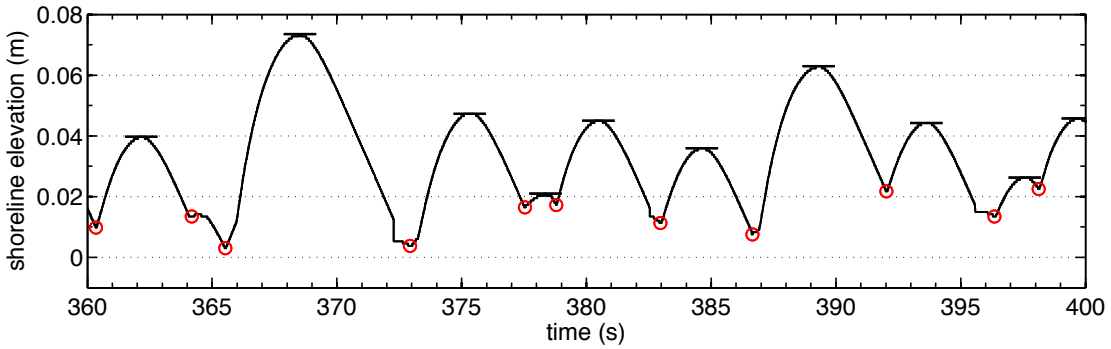

Figure 8: Definition of runup cycles and runup crests or maxima. Runup cycles occur between the minima in the shoreline elevation denoted using circles. Runup crests are identified by the flat lines at the maxima.

4.1.3. Collation of runup statistics

Random realisations of irregular sea states are first obtained by assuming the sea surface to be a Gaussian random variable. A finite wave record is constructed at the paddle by a Fourier summation of wave components using the random-phase random-amplitude method described in Section 3.4. The corresponding linear paddle signal can be obtained using the Biésel transfer function and is corrected by applying a second-order transfer function approximated from the theory of Schäffer (1996). For each random realisation of the spectrum, the paddle domain width (defined as ten times the maximum paddle excursion) and the sponge layer width vary with time.

Free-surface elevation and shoreline position time-histories resulting from the propagation of the incident wave up the beach are computed from the second-order wave generation irregular wave runup simulations. For a given shoreline elevation time-history, the elevation maxima — referred to as runup maxima or crest — are determined as follows. As shown in Figure 8, the minima of the shoreline elevation are first identified (marked with circles in the figure). In most cases successive minima delimit a runup cycle and contain a runup crest (marked by a horizontal line). This definition of the runup cycle is based on the swash cycle definition used by Holman (1986) and Hughes et al. (2010) among others, where the cycle begins when the shoreline begins moving landward and ends when the shoreline retreats to its original position or another wave begins to push the shoreline landward again. It is important to note that the discrete nature of the shoreline (discretised by the finite volume cells) leads to difficulties in defining genuine shoreline maxima and minima. Small motions of the wave front from a wet cell to a dry cell may occur in a region of otherwise constant shoreline elevation. Motions of the shoreline that consecutively wet or dry at least two 'grid' cells are accepted as constituting a genuine shoreline motion. If the amplitude of the motions is less than two cells, then the motion is considered to

be noise. It is for this reason that no runup event is considered to have occurred at time 364 s in Figure 8. However, small swash motions such as those occurring at 378 s and 396 s are counted.

For every random realisation of the prescribed offshore conditions we determine the maximum runup from the shoreline record and so construct a distribution of extreme runup elevations. Each extreme runup value corresponds to the maximum shoreline elevation that occurs during the incidence of (on average) 280 random waves over an interval of 491.52 s. Of course, the number of runup crests from which we choose the maximum value is smaller than the number of offshore waves due to surf zone interactions.

4.2. Statistical analysis of beach runup

The statistical properties of the ensembles of shoreline elevation records are investigated next, with bulk statistics and certain extreme value statistics of the collated runup maxima quantified for each beach slope. Coastal engineers and managers are interested in the extreme runup value in a given period, e.g. the largest runup during a storm, and so of most relevance is the nature of the extreme value distribution of runup maxima. Offshore data are often provided in three-hour segments because the wave statistics, characterised by a certain significant wave height and peak period, tend not to vary much over such an interval. A three-hour wave record from a storm with a typical 10 s zero crossing period will comprise approximately 1000 waves and so the largest runup in 1000 waves is often of interest despite the seemingly arbitrary nature of the threshold. By considering the ensemble of incident sea-state realisations, and associated shoreline motions, we can estimate (qualitatively at least) how often these extreme runup events occur. However, in order to assess the influence of beach slopes on shoreline motion and the driving physical processes, it is useful first to consider the bulk statistics of the local shoreline maxima or runup crests.

4.2.1. Ratio of number of runup crests to incident-wave crests

In a laboratory study of random wave runup Mase (1989) calculated the ratio of number of runup crests to number of incident wave crests, α, for a wide range of beach slopes and incident wave conditions. Mase then proposed an empirical formula for α in terms of the surf similarity parameter (or Iribarren number) $\xi = \tan\beta/\sqrt{H_s/L_0}$, where L_0 is the peak offshore wavelength, having previously shown (Mase and Iwagaki, 1984) that α is governed by this surf similarity parameter alone. A useful preliminary check for the present irregular wave runup model is to examine whether α can be described solely in terms of ξ, following Mase (1989) who estimated α for beach slopes of 1/5, 1/10, 1/20, and 1/30 using a similar flume geometry and incident wave

conditions (water depth 45 cm, tank length 27 m, Pierson-Moskowitz spectrum, peak frequencies ranging from 0.4 Hz to 1.2 Hz) to those in Section 4.1.2. Time series of offshore random waves were generated for different peak spectral frequencies, with observed significant wave heights ranging from 5 cm to 10 cm. The length of the runup and free-surface elevation records in each random wave test corresponded to 650–900 individual waves. The empirical formula for α expressed in terms of the surf similarity parameter (Mase, 1989) is:

$$\alpha = \begin{cases} 0.72\xi^{0.58} & \text{for } \xi \leq 0.91, \\ 0.70\xi^{0.28} & \text{for } 0.91 < \xi \leq 3.57, \\ 1 & \text{for } \xi > 3.57. \end{cases} \tag{3}$$

To implement the check, sea-state ensembles with target significant wave heights H_s ranging from 0.025 m to 0.100 m are investigated on standard beach slopes (1/10, 1/20, 1/40) and an additional slope (1/30). Table 1 lists the full range of incident wave conditions, beach slopes and ensemble averaged α values. Of particular interest are the random wave runup simulations on this 1/30 beach for incident sea state realisations with $H_s = 0.044$ m, giving $\xi = 0.33$ identical to that for a significant wave height $H_s = 0.10$ m on the 1/20 beach slope. Runup for a small ensemble of incident sea states with target $H_s = 0.025$ m on a 1/10 beach slope are also simulated in order to obtain $\xi > 0.91$ for comparison with the second case in the empirical formula in Equation (3). The final case $\xi > 3.57$ corresponds to highly reflective conditions where every incident wave causes a shoreline motion and is therefore not investigated. The incident free-surface elevation offshore of the beach toe is obtained as part of the coupled runup simulation and so the number of waves N_W in the offshore region (specifically at $x = 8.0$ m just offshore of the beach toe) is computed using a zero up-crossing method. By adopting the definition of runup crest from Section 4.1.3 it is straightforward to calculate the number of runup crests and the associated runup crest to wave crest ratio for each sea-state realisation. Empirically predicted values for the ratio of runup crest to wave crest occurrences α_{EMP} are also included in Table 1 for completeness. Uncertainties are estimated using a single standard deviation from the ensemble of values.

Comparison of the values of α computed for cases V and VI in Table 1 confirms that the shoreline motions predicted by the model depend solely on the surf similarity parameter (within the statistical margins of uncertainty). This is despite the incident significant wave height varying by a factor of two for runup on the 1/20 and 1/30 beaches. In both cases, the number of runup crests is slightly less than a half the number of incident waves counted offshore of the beach toe.

Case	M	$\tan\beta$	H_s (m)	ξ	$\langle N_W \rangle$	$\langle N_R \rangle$	$\langle \alpha \rangle = \langle N_R/N_W \rangle$	α_{EMP}
I	16	1/10	0.025	1.33	277 ± 7	247 ± 4	0.89 ± 0.03	0.76
II	16	1/10	0.050	0.94	277 ± 7	237 ± 3	0.86 ± 0.02	0.69
III	30	1/10	0.100	0.67	277 ± 8	214 ± 5	0.78 ± 0.02	0.57
IV	16	1/20	0.050	0.47	277 ± 7	169 ± 6	0.61 ± 0.03	0.47
V	30	1/20	0.100	0.33	277 ± 8	136 ± 6	0.49 ± 0.02	0.38
VI	16	1/30	0.044	0.33	277 ± 7	129 ± 6	0.47 ± 0.03	0.38
VII	16	1/40	0.050	0.24	277 ± 7	98 ± 6	0.36 ± 0.02	0.32
VIII	30	1/40	0.100	0.17	277 ± 8	77 ± 4	0.28 ± 0.02	0.26

Table 1: Ratio α of the number of runup crests N_R to number of incident waves N_W for ensembles of size M, of incident sea-state realisations of different significant wave heights H_s on different beach slopes ($\tan\beta$) corresponding to different surf similarity parameters ξ. Ensemble averages are implied by the notation $\langle\rangle$. α_{EMP} denotes estimates based on Mase's empirical formula (3).

This confirms that our irregular wave runup model captures the surf zone and swash processes observed by Mase and Iwagaki (1984) in a qualitatively correct manner. In physical terms this is explained by the fact that surf zone width (and not just breaker type) depends on incident wave steepness and beach slope according to the surf similarity parameter. The width of the surf zone determines how much bore capture occurs and thus how many shoreline motions occur relative to the number of incident waves. Note that the spectral zero-crossing period is computed to be 1.75 s for the Pierson-Moskowitz spectrum specified in Section 4.1.2. For a repeat period of $T_r = 491.52$ s, this corresponds to 281 waves per repeat period which is consistent with the number of offshore waves counted using the zero up-crossing method (277 ± 7 or 277 ± 8) within the margins of uncertainty of the ensemble averages.

Despite inevitable differences in incident irregular wave field generation (and the absence of reflected wave absorption in the laboratory flume) we compare numerically predicted values of α with those from the empirical formula derived by Mase (1989) in Table 1. Although Mase and Iwagaki (1984) report the spectral shape, peak frequencies and range of test durations, they do not describe the exact method used to generate their wavemaker signals. We therefore assume linear wavemaker theory was employed in conjunction with the random-amplitude/random-phase method. Significant wave height was not prescribed *a priori*; instead it was obtained from the free-surface elevation measurements. Thus, reflected wave contributions were assumed negligible, which may not have been the case for the steepest beaches considered. This is in contrast to the numerical simulation approach where the significant wave height H_s is prescribed beforehand and serves as an input parameter to the paddle motions creating the incident wave-field. Identification of runup crests from numerical and experimental shoreline elevation time-histories might also

lead to discrepancies. The numerical results in Table 1 overestimate the ratio of the number of runup crests to offshore incident wave crests compared to the empirical formula based on the experimental data by approximately 20% for all but the gentlest beach slope. Several factors underlie the disparity in the number of runup maxima observed. Small runup crests identified from simulated runup time histories using the criterion illustrated in Figure 8 may not have been identified or be visible in the laboratory measurements of Mase (1989). Furthermore, absence of second-order correction to the laboratory paddle motion and the presence of re-reflected waves from the paddle in the laboratory flume would also cause differences between the numerical and experimental incident wave fields.

We demonstrate the effect of these discrepancies by comparing runup due to an incident irregular wave field generated by first-order wavemaker motions with a very weak generating-absorbing sponge layer in the offshore region (numerical instabilities develop in the complete absence of a sponge layer) to runup obtained from the corresponding second-order corrected signal with standard sponge layer generation-absorption. Figure 9 shows extracts of the shoreline elevation time-histories for each beach slope. This figure strikingly illustrates the reduction in number of runup crests as the beach slope becomes gentler, despite the same incident wave conditions at each beach toe (Figure 9 (d)). A substantial increase occurs in the magnitude of runup events on all slopes, due to the combined effects of linear wave generation and a weak sponge layer. For the steepest beach slope, the total number of runup maxima for the linear wave generation case with a weak sponge layer is 197, a 9% reduction in the number of crests. Although not accounting completely for the discrepancy between experiment and numerical incident wave fields, these findings do illustrate the importance of implementing second-order corrected wavemaker theory and long wave reflection.

4.2.2. Extreme runup distributions

Each shoreline elevation record corresponds to the propagation of approximately 280 incident waves from the paddle to beach, based on the mean zero up-crossing period of the underlying spectrum. A reasonable estimate for the mean zero up-crossing period at full scale is $T_z = 8.0\,\mathrm{s}$ and thus the time record corresponds to about 37 minutes of data. This duration is of similar order of magnitude to those of the free-surface elevation wave records used to characterise a sea state and similar to the runup record length considered in the extreme value statistical analysis by Holman (1986). Note that this record length, which equals one repeat period of the discretised offshore wave energy density spectrum, has been chosen somewhat arbitrarily. A

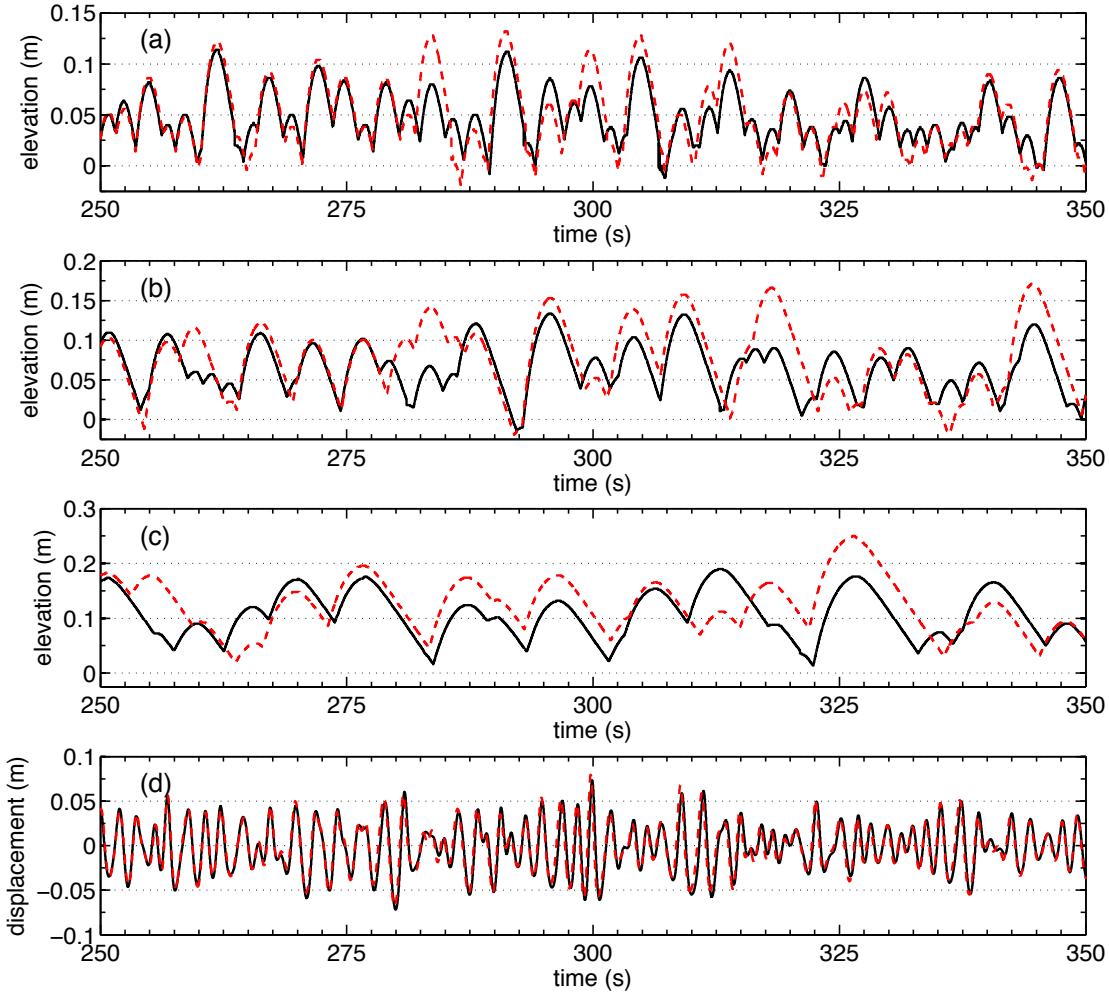

Figure 9: Time histories of (a—c) shoreline elevations and (d) free-surface elevation (with the incident wave at the beach toe) for sea-state realisation I in Table 1 obtained using the linear paddle signal with a weak sponge layer (red, dashed) and the second-order corrected paddle signal with a standard sponge layer (black) for beach slopes (a) 1/10, (b) 1/20, (c) 1/40.

different discretisation of the energy spectrum would yield a different repeat period. Nevertheless, the records may be sub-divided or combined to form smaller or larger sample sizes from which to obtain the maximum runup elevation. We analyse the statistics for the maximum predicted runup elevation in a single wave record and sets of two combined wave records.

In the following we examine distributions of runup maxima for evidence of an upper limit for runup. For each bed slope, simulations of wave runup have been conducted for 100 random realisations of the incident sea state. Maximum runup elevations from each of the shoreline records of one repeat period in duration are then collated to yield an extreme-value type distribution comprising 100 samples. Note that the number of runup maxima (from which the extreme value is selected) in each shoreline elevation record varies according to the beach slope — for the 1/10 slope, 1/20 slope and the 1/40 slope the number of runup maxima will be approximately 80%, 50% and 30% of the number of incident waves, respectively. Thus, in terms of extreme value statistics, the distributions are not exactly equivalent. Nevertheless, in the context of coastal (and ocean) engineering the return period of a runup maximum for a given set of offshore conditions will be of substantial interest, and so it is more consistent to consider the same time interval of wave incidence for each beach slope. As noted by Holman (1986), the fitting of an extreme value frequency distribution to a relatively small set of data points creates large uncertainties in the details of the upper tail. The return period of a 'rare event' can be derived from the tail of an extreme value distribution; however, it is very sensitive to the tail shape and so we do not seek to obtain such an estimate. Instead, a comparison between the distribution shapes of the maximum runup crest occurring in the shoreline elevation time records is presented for each of the three beach slopes. Figure 10 shows the distribution of the maximum runup crests obtained from shoreline elevation records of one full repeat period in length for each beach slope. In each case there appears to be a smaller secondary peak in the upper tail of the distributions. This may imply the existence of an upper limit to the maximum runup crest values.

For the 1/20 beach slope, the secondary peak at the upper tail is followed by a sharp drop-off in the probability distribution to zero beyond values of 0.084 m, again indicating runup saturation. Such a steep drop-off in the probability distribution is less obviously apparent for the steepest beach of slope 1/10 although saturation does appear to occur at 0.140 m. This distribution of maxima has a 'heavy' upper tail with a number of the maximum runup elevations occurring quite far from the mean compared to the smallest maximum runup elevations. Note that the 'width' of the distribution is approximately 0.04 m in this case, 0.025 m for the 1/20 beach and 0.015 m for the 1/40 beach — the x-axes of the histograms are scaled differently. For the gentlest

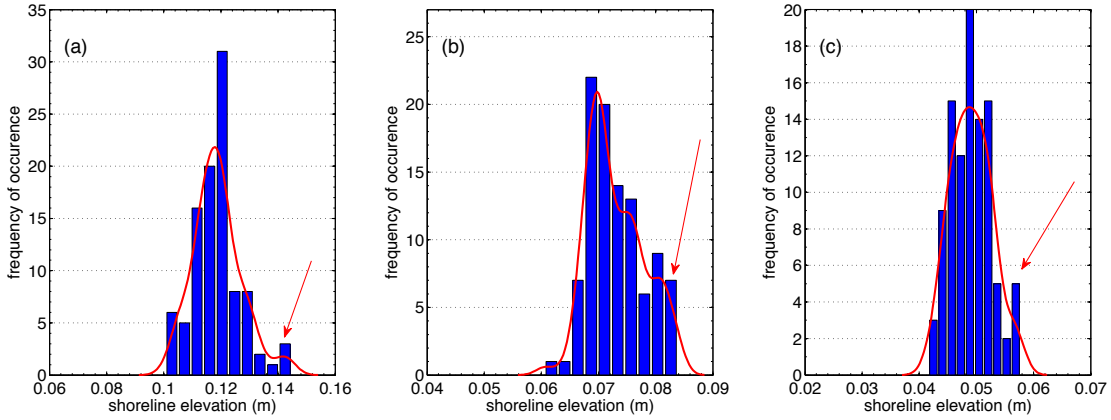

Figure 10: Distribution of maximum runup crest values obtained from shoreline elevation time records comprising 280 offshore waves for beach slopes of (a) 1/10, (b) 1/20, and (c) 1/40. Red arrows indicates the position of the ensemble maximum in each case.

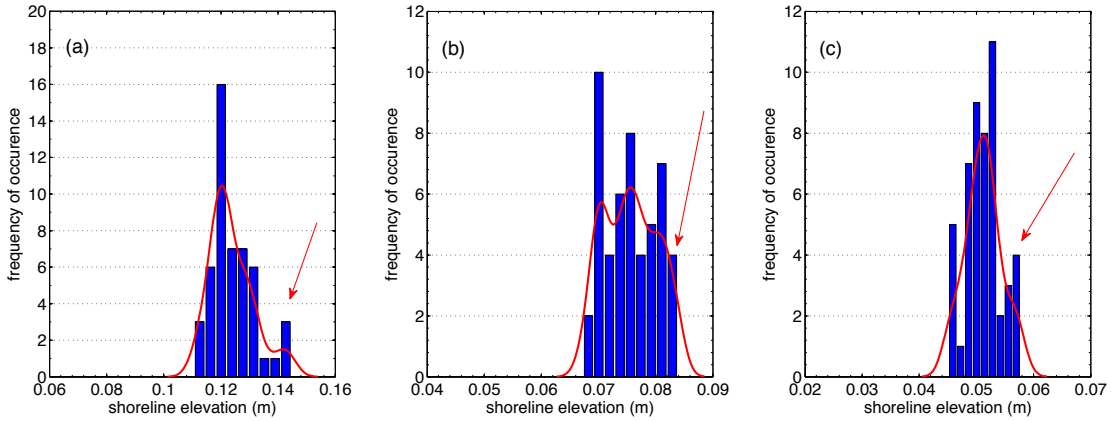

Figure 11: Distribution of maximum runup crest values obtained from shoreline elevation time records comprising 560 offshore waves for beach slopes of (a) 1/10, (b) 1/20, and (c) 1/40. Red arrows indicates the position of the ensemble maximum in each case.

(1/40) beach slope, the distribution of the maximum runup crest values is quite narrow and almost symmetric, with the upper tail having a slightly greater spread than the lower tail. The presence of an upper limit to the maximum runup crests is visible in the distribution of maximum runup values for the ensemble of fifty shoreline elevation records comprising 560 incident waves (obtained by combining two standard shoreline elevation records) as shown in Figure 11. It might be anticipated that evidence of an upper limit to runup would become clearer for ensembles of longer shoreline records; however, the smoothness of the distributions is then limited by the reduced number of samples.

4.2.3. Saturation in swash spectra

Evidence of runup saturation in certain frequency bands has been observed by many authors when analysing swash spectra on gently sloping beaches. Raubenheimer and Guza (1996) investigated swash saturation on beaches with intermediate slopes while Ruessink et al. (1998) and Ruggiero et al. (2004) investigated swash saturation observed in data sets collected on dissipative natural beaches. Saturation was assessed by examining the properties of swash or run-up energy density spectra obtained from the field measurements and by investigating the correlation of infragravity or sea swell swash heights with beach slope and/or offshore significant wave height. Ruessink et al. (1998) averaged the measured runup data in the alongshore direction whereas Ruggiero et al. (2004) considered measurements along each transect of the beach independently giving a range of runup data for different beach slopes. In many of the field studies reported in the literature, it is difficult to isolate the dependence of swash on one particular environmental condition (e.g. beach slope or offshore significant wave height) due to continuous changes in these conditions.

Using the numerical wave flume modified to model irregular wave runup described in this paper, we are able to construct large runup data sets from which reliable swash statistics can be obtained for any permutation of environmental conditions. Therefore, we can investigate the dependence of swash on any given factor by holding all other conditions constant. To demonstrate this capability, swash spectra on each slope are determined from ensembles of 16 runup records on each of three representative beach slopes (1/10, 1/20, 1/40) for two different offshore significant wave heights (0.05 m and 0.10 m) and compared in Figure 12. Note that a sub-sample of 16 records has been chosen from the full ensemble of 100 runup records for the $H_s = 0.10$m cases so that each ensemble-averaged swash spectrum is equivalent. Ensemble-averaged swash energy density spectra are obtained in two ways: first, using a direct FFT of the shoreline elevation

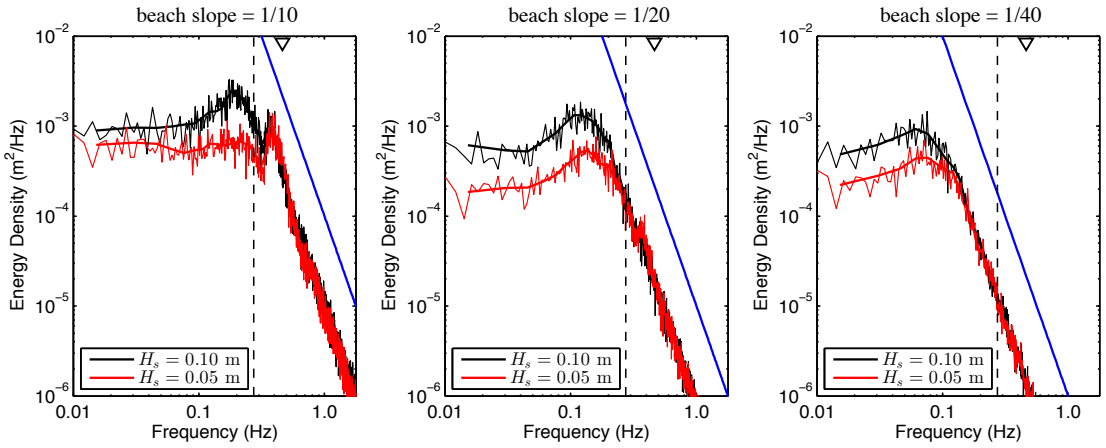

Figure 12: Swash spectra for reflective, intermediate, and dissipative beaches of slope 1/10, 1/20, and 1/40, respectively, for incident significant wave heights of $H_s = 0.05$ m (red) and $H_s = 0.10$ m (black). Blue solid lines indicate $f^{-}4$ dependence in the log-log space and the black triangle indicates the peak frequency of the incident spectrum.

time histories and secondly, using Welch's power spectral density estimate with zero overlap and an averaging factor of 8 (see documentation of the pwelch function in Matlab®). Thick lines in Figure 12 indicate the averaged power spectral density estimate and are smoother than the direct FFT approach (thin lines). The dashed black line in each log-log plot indicates the estimate for the division between the infragravity and sea swell frequency bands at 'experimental' scale. At full scale, this threshold is 0.05 Hz and by assuming offshore depths of 15 m in the field (Ruessink et al., 1998), the corresponding value for a numerical wave flume of depth 0.5 m is obtained.

A variety of interesting swash behaviours is evident in Figure 12. Spectral roll-off proportional to f^{-4} is clearly observed for all beach slopes. However, as noted by Mase (1988) this may be largely due to the parabolic nature of the runup time histories as illustrated in Figure 8. Swash spectra for steeper beach slopes are shifted towards higher frequencies than spectra for gentler slopes, consistent with observations in the field by Ruggiero et al. (2004). Saturation of runup, identified in Figure 12 as where the swash spectra for the two different offshore significant wave heights are equal, is observed to occur for lower frequencies for the gentler beach slopes. In particular, on the dissipative beach the saturated portions of the spectra extend a significant distance into the infragravity band, as observed by Ruessink et al. (1998) and Ruggiero et al. (2004).

The occurrence of saturation in the sea swell band for the reflective beach is notable in Figure 12. Two peaks in the swash spectra are observed for this relatively steep beach slope, one in the sea swell band and one in the infragravity band. The spectral peak in the sea swell

band for offshore wave heights $H_s = 0.05$ m and $H_s = 0.10$ m occurs at approximately at 0.40 Hz and 0.36 Hz, corresponding to swash periods of 2.5 s and 2.8 s respectively. Swash periods can be estimated from Table 1 using T_p/α (where $T_p = 1/f_p = 2.16$ s) and are approximately 2.5 s and 2.8 s for the relevant cases II and III. Saturation of sea swell swash has occurred on the reflective beach. However, larger swash excursions due to increased infragravity energy remain possible for larger incident significant wave heights. Evidence of a secondary peak in the sea swell band is present for the intermediate beach. Only for the dissipative beach does all incident wave energy appear to have been down-shifted to the infragravity band.

4.2.4. Influence of 'precursor' waves on total runup

It is well known that the properties of preceding waves and the size of resultant backswash can have a substantial influence on subsequent swash motions. We therefore now investigate the number of preceding waves required in order to yield accurate shore conditions preceding the arrival of a prescribed incident wave group. Given the importance of extreme runup events, a particularly large wave runup crest from the ensemble of irregular wave runup simulations for the 1/20 beach slope is first considered. In Figure 13, the origin of the time axes is specified to coincide with the occurrence of the extreme runup event and so waves, bores, and shoreline motions can be identified relative to this extreme event; however, in the actual simulation the event occurs after more than 450 s. The analysis is also repeated for large runup events on the beaches with steeper (1/10) and gentler (1/40) slopes. The number of precursor waves necessary to obtain the same shoreline dynamics as the fully-established irregular wave runup simulation depends on the length of the inherent 'memory' in the dynamics of runup on the particular beach in question.

To quantify the effect of preceding waves on the extreme runup crest, a series of simulations are conducted with progressively fewer waves preceding the arrival of the main group yielding the large runup event, and the corresponding shoreline elevations compared. The precise effect of each incident wave on shoreline elevation is not easily quantified due to the bore-bore interactions in the surf zone (e.g. large bore 'capture of smaller bores). Establishment of a one-to-one correspondence between offshore waves and runup crests is not possible. Nonetheless, comparison of shoreline time-histories for simulations with fewer sets of waves arriving at the shore prior to the extreme run-up event should provide an estimate as to how many preceding waves are necessary to represent fully an extreme runup event. In order to control the number of 'precursor' waves arriving at the shore immediately before an extreme runup event, an absorbing sponge layer

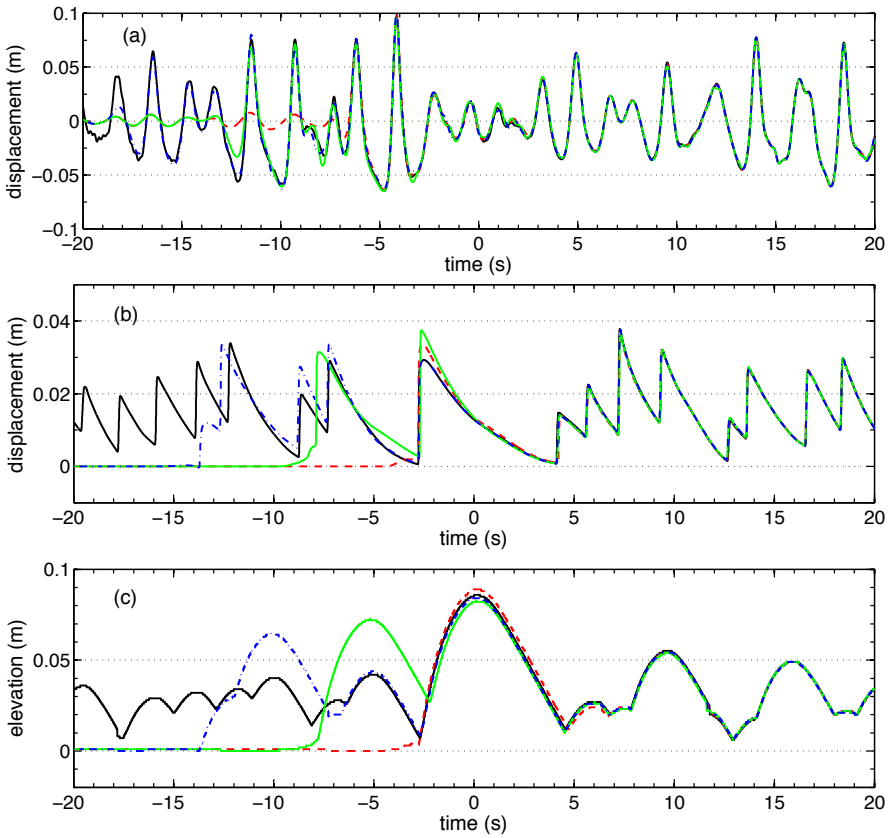

Figure 13: Time-histories of free-surface displacement at (a) the mid-point $x = 13.33m$ of the beach, and (b) the still water shoreline position and (c) the moving shoreline elevation relative to still water level for the beach sponge layer damping strength decaying to zero one repeat period (black), 19.5 s (blue, dash-dot), 14.25 s (green), and 9.0 s (red-dashed) before the maximum runup occurs (see web version for colour).

spanning the entire beach is included in the runup simulation. With reference to Figure 2, an absorbing sponge layer similar to that in the incident wave simulation is imposed from beach toe to shore in the runup simulation. Incident waves steadily decay to zero over the sponge layer and the initial damping strength is specified so that no shoreline motions occur. To allow a certain number of waves to arrive at the shore prior to the extreme runup event we simply ramp the sponge layer strength to zero at the appropriate time.

Figure 13 presents time-histories of free-surface displacement at the mid-point of the beach, at the still water shoreline, and shoreline elevations (with respect to SWL) for four simulations involving decreasing numbers of precursor waves (including a full repeat period of incident waves) before the occurrence of the extreme runup event. Convergence to the fully established shoreline motions depends on the number of waves reaching the shore prior to the arrival of the set of waves causing a large runup event. The number of undamped waves arriving at the shore in turn depends on time of flight of the waves from the beach toe to the (still water) shoreline. The first bore to arrive at the shore after the sponge layer is 'removed' may incorporate several of the damped, reduced amplitude waves that are present in the absorbing sponge layer prior to its removal. Consequently, to select the time at which to remove the absorbing sponge layer so that the first waves to reach the shore are those forming the extreme runup bore requires subjective judgement (based on the time of flight estimate). By ramping the sponge layer strength to zero (with ramp duration $T_z/2$ as standard) 9.0 s before the maximum runup event, the first significant waves to arrive at the shore form extreme runup bore, as shown by the red-dashed line in Figure 13 (referred to as runup case A). The duration of a compact focused wave group, typically comprising three large wave crests in a Pierson-Moskowitz sea state, is approximately equal to three mean zero up-crossing periods ($3T_z = 5.25$ s). Thus, by reducing the sponge layer strength to zero at times 14.25 s (runup case B) and 19.5 s (runup case C) before the extreme runup event, we can allow approximately three and six waves or one and two wave groups, respectively, to arrive at the shore just before the main bore. In this manner, the effect of the preceding bores or 'precursor' waves on the subsequent shoreline motions is investigated. The same analysis is repeated for an extreme runup event on the 1/10 and 1/40 beaches (albeit with different time of flight estimates).

Figure 13(b, c) shows that both the free-surface elevation at the still water shoreline and the shoreline elevation in runup case A are over-predicted compared to the corresponding elevations that occur as the fully-established irregular wave train arrives at the shore. In Figure 13(a), the wave crests at the mid-point of the beach which occur (approximately) at times $t = -6$ s and $t = -4$ s must comprise the main components of the large bore causing extreme runup as they are

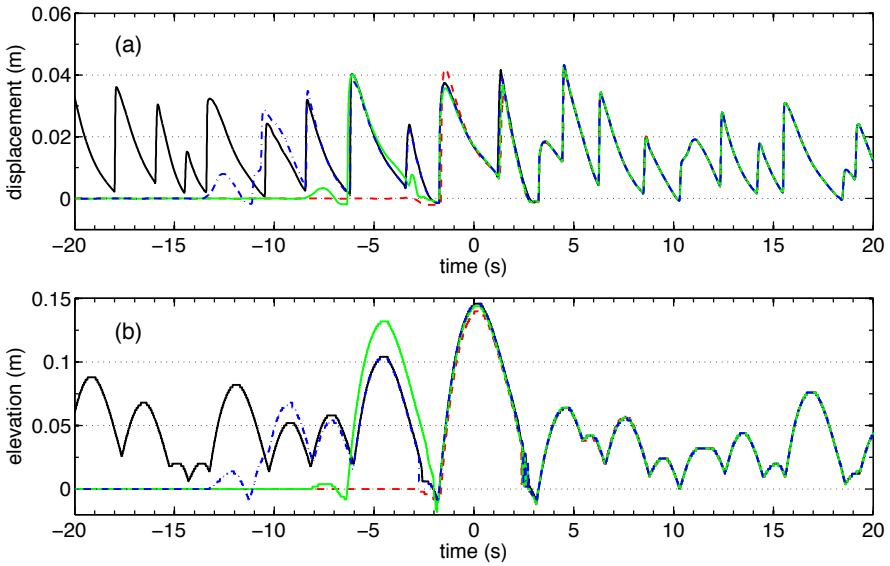

Figure 14: Time-histories of free-surface displacement at (a) the still water shoreline position and (b) the moving shoreline elevation relative to still water level on the 1/10 beach for the beach sponge layer damping strength decaying to zero one repeat period (black), 14.70 s (case C; blue, dash-dot line), 9.45 s (case B; green line), and 4.20 s (case A; red-dashed line) before the maximum runup occurs (see web version for colour).

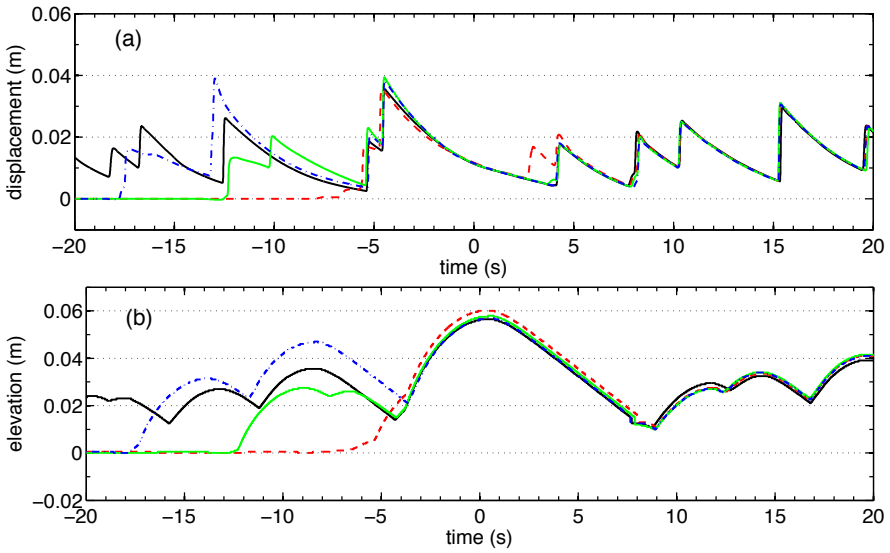

Figure 15: Time-histories of free-surface displacement at (a) the still water shoreline position and (b) the moving shoreline elevation relative to still water level on the 1/40 beach for the beach sponge layer damping strength decaying to zero one repeat period (black), 29.50 s (case C; blue, dash-dot line), 24.25 s (case B; green line), and 19.0 s (case A; red-dashed line) before the maximum runup occurs (see web version for colour).

the first waves fully reproduced in case A. The two following wave crests are fully propagated in case B (where the sponge layer is removed at time $t = -14.25\,\mathrm{s}$) and, in the absence of precursor waves at the shore, lead to a large runup event (at $t = -5.0\,\mathrm{s}$) also. However, the rundown or backswash occurring after the runup event at $t = -5.0\,\mathrm{s}$ in case B appears to impede the propagation of the main bore up the beach and results in a smaller predicted maximum runup elevation. Nevertheless, the free-surface elevation at the still water shoreline is still over-predicted relative to the free-surface elevation of the fully-established irregular wave train at the shore. Runup case C, allowing approximately six fully-formed waves to propagate past the mid-point of the beach leading to three bore motions at the still water shoreline, provides the best agreement with the shoreline dynamics as shown in Figure 13(b) and (c).

Figures 14 and 15 compare moving shoreline elevations and still water shoreline free-surface displacements around an extreme runup event for different numbers of precursor waves on the 1/10 and 1/40 beaches, respectively. Shoreline motions for case A comprising the extreme bore motion only with no precursor waves approximate the actual extreme shoreline excursion reasonably well with relative differences compared with fully established shoreline excursions of just less than 10%. Improved agreement is achieved in cases B and C where one and two wave groups are allowed to precede the wave group causing the extreme bore motion. This is particularly evident on 1/10 beach slope where both the extreme bore motion and the preceding bore motion are almost exactly reproduced by Case C where two precursor wave groups are allowed to arrive at the shore. In fact, on the reflective 1/10 beach slope only one precursor wave group is necessary to precondition the shore so that that the following bore motion is accurately reproduced. On the 1/40 beach, it appears that one precursor wave group (case B) is also sufficient although the reproduction of the bore motions at the still water shoreline is not as accurate as for the 1/10 beach.

In all cases, the maximum shoreline elevation is reasonably well approximated by incident wave trains which, after passage through the surf zone, yield just the main bore. Better agreement is achieved by including a precursor wave group (approximately three waves) with the main incident wave train which preconditions the shoreline to resemble the fully established shoreline conditions. Even on the gentlest slopes where the surf zone is longest and swash zone interactions may be significant, a single precursor wave group appears to lead to an excellent approximation of the extreme shoreline motion.

5. Conclusions

A coupled incident-runup model based on a hybrid 1DH Boussinesq-NLSW solver incorporating a generating-absorbing sponge layer was used to create long duration simulations of unidirectional irregular wave runup on uniform, gently sloping beaches. The generating-absorbing sponge layer facilitated simultaneous propagation of incident irregular waves and absorption of outgoing reflected waves. The offshore incident wave field was first simulated in a domain without the beach present. Incident and runup solutions were then coupled by imposing the incident wave solution on the sponge layer in the runup simulation at each time-step. An in-built moving piston paddle allowed accurate generation of incident waves to second order; it is essential to include correctly the subharmonic component for accurate runup and overtopping modelling (as previously demonstrated by Orszaghova et al. (2014)). Convincing evidence of the need to absorb reflected waves was demonstrated by comparing shoreline motions for two coupled simulations involving the tuned sponge layer strength and negligible sponge layer strength (approximating zero absorption).

Statistics of runup maxima for irregular wave incidence (with approximately correct second-order bound wave structure) on beaches of three different slopes were compiled from a large ensemble of long irregular wave runup simulations. The beach slopes corresponded to reflective, intermediate, and dissipative beach types. Comparison between the predicted ratio of number of wave runup crests to number of offshore wave crests and corresponding results from an empirical formula derived by Mase (1989) for random wave runup in a laboratory wave flume revealed certain discrepancies due in part to differences in the incident wave fields. However, this ratio was shown to be governed by the Iribarren number alone, in accordance with Mase's findings. In qualitative terms, the runup statistics for the various beach slopes indicated that the 1DH hybrid model was capable of reproducing efficiently the important surf zone interactions for runup on plane beaches.

Swash spectra for each of the beach slopes were obtained for two offshore significant wave heights. Significant differences in the spectral forms were observed. In particular, an obvious peak in the sea swell frequency band was evident only for the steepest (reflective) beach. Saturation of swash penetrated farthest into the infragravity frequency band for the bed slope representing a dissipative beach. High frequency spectral roll-off proportional to f^{-4} was also observed in accordance with many field studies. Distributions of runup maxima from each of the time-varying shoreline elevation records were compiled and examined. Secondary peaks in the upper tails of

the distributions suggested the existence of an upper limit for extreme runup. Analysis of a single extreme runup event highlighted the importance of 'pre-conditioning' the bore motion at the shore.

Acknowledgements

This work was conducted within the ENFORCE (Extreme Responses using NewWave: Forces, Overtopping and Runup in Coastal Engineering) project, under EPSRC Grant EP/K024108/1.

References

Baldock, T., Holmes, P., Bunker, S., Weert, P. V., 1998. Cross-shore hydrodynamics within an unsaturated surf zone. Coastal Engineering 34 (3—4), 173 – 196.
URL http://www.sciencedirect.com/science/article/pii/S0378383998000179

Barthel, V., Mansard, E., Sand, S., Vis, F., 1983. Group bounded long waves in physical models. Ocean Engineering 10 (4), 261 – 294.
URL http://www.sciencedirect.com/science/article/pii/0029801883900124

Bingham, H. B., Agnon, Y., 2005. A Fourier–Boussinesq method for nonlinear water waves. European Journal of Mechanics - B/Fluids 24 (2), 255 – 274.
URL http://www.sciencedirect.com/science/article/pii/S0997754604000688

Borthwick, A. G. L., Hunt, A. C., Feng, T., Taylor, P. H., Stansby, P. K., 2006. Flow kinematics of focused wave groups on a plane beach in the U.K. Coastal Research Facility. Coastal Engineering 53 (12), 1033 – 1044.
URL http://www.sciencedirect.com/science/article/pii/S0378383906000950

Chen, Q., 2006. Fully nonlinear boussinesq-type equations for waves and currents over porous beds. Journal of Engineering Mechanics 132 (2), 220–230, cited By 22.
URL http://www.scopus.com/inward/record.url?eid=2-s2.0-30944464287&partnerID=40&md5=7ac55ba8a9604b939ce4c9df68df78e6

Green, A. E., Naghdi, P. M., 11 1976. A derivation of equations for wave propagation in water of variable depth. Journal of Fluid Mechanics 78, 237–246.
URL http://journals.cambridge.org/article_S0022112076002425

Guza, R. T., Thornton, E. B., 1982. Swash oscillations on a natural beach. Journal of Geophysical Research: Oceans 87 (C1), 483–491.
URL http://dx.doi.org/10.1029/JC087iC01p00483

Higuera, P., Losada, I. J., Lara, J. L., 2015. Three-dimensional numerical wave generation with moving boundaries. Coastal Engineering 101 (0), 35 – 47.
URL http://www.sciencedirect.com/science/article/pii/S0378383915000666

Holman, R., 1986. Extreme value statistics for wave run-up on a natural beach. Coastal Engineering 9 (6), 527 – 544.
URL http://www.sciencedirect.com/science/article/pii/0378383986900025

Hughes, M. G., Moseley, A. S., Baldock, T. E., 2010. Probability distributions for wave runup on beaches. Coastal Engineering 57 (6), 575 – 584.
URL http://www.sciencedirect.com/science/article/pii/S0378383910000025

Hunt, A. C., 2003. Extreme Waves, Overtopping and Flooding at Sea Defences. Ph.D. thesis, University of Oxford.

Hunt-Raby, A. C., Borthwick, A. G., Stansby, P. K., Taylor, P. H., 2011. Experimental measurement of focused wave group and solitary wave overtopping. Journal of Hydraulic Research 49 (4), 450–464.

Israeli, M., Orszag, S. A., 1981. Approximation of radiation boundary conditions. Journal of Computational Physics 41, 115–135.

Larsen, J., Dancy, H., 1983. Open boundaries in short wave simulations – a new approach. Coastal Engineering 7, 285–297.

Madsen, P., Sørensen, O., 1993. Bound waves and triad interactions in shallow water. Ocean Engineering 20 (4), 359 – 388.
URL http://www.sciencedirect.com/science/article/pii/002980189390002Y

Madsen, P., Sørensen, O., Schäffer, H., 1997a. Surf zone dynamics simulated by a boussinesq type model. part i. model description and cross-shore motion of regular waves. Coastal Engineering 32 (4), 255 – 287.
URL http://www.sciencedirect.com/science/article/pii/S0378383997000288

Madsen, P., Sørensen, O., Schäffer, H., 1997b. Surf zone dynamics simulated by a Boussinesq type model. Part II: surf beat and swash oscillations for wave groups and irregular waves. Coastal Engineering 32 (4), 289 – 319.
URL http://www.sciencedirect.com/science/article/pii/S037838399700029X

Madsen, P. A., Murray, R., Sørensen, O. R., 1991. A new form of the Boussinesq equations with improved linear dispersion characteristics (Part 1). Coastal Engineering 15, 371–388.

Madsen, P. A., Sørensen, O. R., 1992. A new form of the Boussinesq equations with improved linear dispersion characteristics. Part 2. a slowly-varying bathymetry. Coastal Engineering 18, 183–204.

Mase, H., 1988. Spectral characteristics of random wave run-up. Coastal Engineering 12 (2), 175–189.

Mase, H., 1989. Random wave runup height on gentle slope. Journal of Waterway, Port, Coastal, and Ocean Engineering 115 (5), 649–661.
URL http://dx.doi.org/10.1061/(ASCE)0733-950X(1989)115:5(649)

Mase, H., Iwagaki, Y., 1984. Run-up of random waves on gentle slopes. Coastal Engineeering Proceedings 1 (19), issn: 2156-1028.
URL https://icce-ojs-tamu.tdl.org/icce/index.php/icce/article/view/382

Orszaghova, J., 2011. Solitary waves and wave groups at the shore. Ph.D. thesis, University of Oxford.
URL http://ora.ox.ac.uk/objects/uuid:5b168bdc-4956-4152-a303-b23a6067bf42

Orszaghova, J., Borthwick, A. G. L., Taylor, P. H., Jan. 2012. From the paddle to the beach - a Boussinesq shallow water numerical wave tank based on Madsen and Sørensen's equations. J. Comput. Phys. 231 (2), 328–344.
URL http://dx.doi.org/10.1016/j.jcp.2011.08.028

Orszaghova, J., Taylor, P. H., Borthwick, A. G., Raby, A. C., 2014. Importance of second-order wave generation for focused wave group run-up and overtopping. Coastal Engineering 94 (0), 63 – 79.
URL http://www.sciencedirect.com/science/article/pii/S0378383914001598

Raubenheimer, B., Guza, R. T., 1996. Observations and predictions of run-up. Journal of Geophysical Research: Oceans 101 (C11), 25575–25587.
URL http://dx.doi.org/10.1029/96JC02432

Raubenheimer, B., Guza, R. T., Elgar, S., Kobayashi, N., 1995. Swash on a gently sloping beach. Journal of Geophysical Research: Oceans 100 (C5), 8751–8760.
URL http://dx.doi.org/10.1029/95JC00232

Ruessink, B. G., Kleinhans, M. G., van den Beukel, P. G. L., 1998. Observations of swash under highly dissipative conditions. Journal of Geophysical Research: Oceans 103 (C2), 3111–3118.
URL http://dx.doi.org/10.1029/97JC02791

Ruggiero, P., Holman, R. A., Beach, R. A., 2004. Wave run-up on a high-energy dissipative beach. Journal of Geophysical Research: Oceans 109 (C6), n/a–n/a, c06025.
URL http://dx.doi.org/10.1029/2003JC002160

Schäffer, H. A., 1996. Second-order wavemaker theory for irregular waves. Ocean Engineering 23 (1), 47 – 88.
URL http://www.sciencedirect.com/science/article/pii/002980189500013B

Shi, F., Kirby, J. T., Harris, J. C., Geiman, J. D., Grilli, S. T., 2012. A high-order adaptive time-stepping {TVD} solver for Boussinesq modeling of breaking waves and coastal inundation. Ocean Modelling 43–44 (0), 36 – 51.
URL http://www.sciencedirect.com/science/article/pii/S1463500311002010

Siddorn, P. D., 2012. Efficient numerical model of wave-structure interaction. Ph.D. thesis, University of Oxford.
URL http://ora.ox.ac.uk/objects/uuid:de36bd2f-cd23-4f11-b67f-9d8cd48ecd3c

Spinneken, J., Swan, C., 2009. Second-order wave maker theory using force-feedback control. part i: A new theory for regular wave generation. Ocean Engineering 36 (8), 539 – 548.
URL http://www.sciencedirect.com/science/article/pii/S0029801809000213

Tissier, M., Bonneton, P., Marche, F., Chazel, F., Lannes, D., 2012. A new approach to handle wave breaking in fully non-linear Boussinesq models. Coastal Engineering 67 (0), 54 – 66.
URL http://www.sciencedirect.com/science/article/pii/S0378383912000749

Tonelli, M., Petti, M., 2012. Shock-capturing Boussinesq model for irregular wave propagation. Coastal Engineering 61 (0), 8 – 19.
URL http://www.sciencedirect.com/science/article/pii/S0378383911001815

Tucker, M., Challenor, P., Carter, D., 1984. Numerical simulation of a random sea: a common error and its effect upon wave group statistics. Applied Ocean Research 6 (2), 118 – 122.
URL http://www.sciencedirect.com/science/article/pii/0141118784900506

Wei, G., Kirby, J., 1995. Time-dependent numerical code for extended Boussinesq equations. Journal of Waterway, Port, Coastal, and Ocean Engineering 121, 251–261.

Wei, G., Kirby, J. T., Sinha, A., 1999. Generation of waves in Boussinesq models using a source function method. Coastal Engineering 36 (4), 271 – 299.
URL http://www.sciencedirect.com/science/article/pii/S0378383999000095

Zhang, Y., Kennedy, A. B., Panda, N., Dawson, C., Westerink, J. J., 2014. Generating-absorbing sponge layers for phase-resolving wave models. Coastal Engineering 84 (0), 1 – 9.
URL http://www.sciencedirect.com/science/article/pii/S0378383913001750